Ocean Engineering 355 (2026) 125205

Contents lists available at ScienceDirect

Ocean Engineering

journal homepage: www.elsevier.com/locate/oceaneng

Research paper

Applicability of predicted cone penetration test profiles from geostatistical co-simulation on deterministic and probabilistic monopile foundation design for offshore wind turbines

Lennart Siemann [a,*], Sigrid Wilhelm [b], Pedram Masoudi [c], Ramiro Relanez [a], Patrick Arnold [b], Benjamin Schwarz [a], Frank Rackwitz [d], Tobias Mörz [e]

[a] Fraunhofer Institute for Wind Energy Systems IWES, Am Fallturm 1, D-28359, Bremen, Germany
[b] GuD Geotechnik und Dynamik Consult GmbH, Darwinstr. 13, D-10589, Berlin, Germany
[c] Geovariances a Datamine Company, 44 avenue de Valvins, F-77210, Avon, France
[d] Chair of Soil Mechanics and Geotechnical Engineering, Technical University of Berlin, Gustav-Meyer-Allee 25, D-13355, Berlin, Germany
[e] UBC Uni Bremen Campus GmbH, Universitätsallee 11–13, D-28359, Bremen, Germany

A R T I C L E I N F O

Keywords:
Predicted CPT
Reliability-based pile design
Offshore wind
Site characterization
Multivariate modelling
Probabilistic
Monopile

A B S T R A C T

To reduce site investigation costs for site characterization as well as timelines in offshore windfarm development, methods to predict the soil profile and essential geotechnical parameters at unexplored locations gain increasing interest from the industry. Hereby, the more abundant geophysical data can be used as guiding information in addition to the scarcely spaced direct investigations to improve the prediction of ground conditions and reduce its uncertainty at unexplored locations. However, since it is a rather new tool in offshore wind site characterization, little is known about the applicability of those predicted soil profiles and the associated geotechnical parameters for the design process of offshore wind infrastructures.

This study aims to highlight the generation of predicted geotechnical profiles and parameters in the form of predicted cone penetration tests (pCPTs) and its use for the design of monopile foundations. Using real data from a German North Sea site the pCPTs are generated by applying geostatistical co-simulation, resulting in a best estimate with a location and depth specific uncertainty. These probabilistic results are utilized for the derivation of a design pile length. This pile length is either computed based on a deterministic estimate of the pCPT, taken as a quantile values, or with a reliability-based approach with respect to a target reliability level. It could be shown that a safe design length in comparison to the measured values is achieved by using a quantile value of 5% or less within a deterministic design or the reliability-based design approach.

1. Introduction

To minimize risk in offshore wind farm development, precise understanding of the subsurface is essential, especially in formerly glaciated margins, as among others encountered in the North and Baltic Sea. This leads to an increasing demand for reliable ground models, with a growing interest in employing quantitative approaches like the prediction of geotechnical parameters using geotechnical and seismic data to shorten development timelines and costs.

Common practice in offshore windfarm site investigation is to perform 2D or 3D seismic data acquisition in a relatively dense grid, together with geotechnical campaigns, i.e. using cone penetration testing (CPT) or borehole investigations. For offshore sites usually large distances are encountered between geotechnical site investigation locations, making the use of the more abundant seismic data indispensable to properly understand geological conditions in between directly explored locations.

As a rather new technique in offshore wind farm site investigation, compared to the conventional geophysical and geotechnical investigations, predicted geotechnical parameters become an increasingly common tool to support site characterization and decision making for offshore infrastructure installation and design. The prediction of geotechnical parameters - mostly in the form of predicted CPT (pCPT) – aims to target not directly explored locations to replace or support in-

* Corresponding author. Fraunhofer Institute for Wind Energy Systems IWES, Am Fallturm 1, D-28359, Bremen, Germany.
E-mail address: lennart.siemann@iwes.fraunhofer.de (L. Siemann).

https://doi.org/10.1016/j.oceaneng.2026.125205
Received 26 September 2025; Received in revised form 5 December 2025; Accepted 19 March 2026
Available online 23 March 2026

situ measurements to build a 2D or 3D ground model. The acquired geotechnical site investigation data provides only discrete information of the site under investigation, while the prediction, especially when incorporating seismic data, allows for a continuous and site wide evaluation. Most common technologies to predict geotechnical parameters are machine learning (ML) algorithms or geostatistical methods. An overview of different methods to predict geotechnical parameters (i.e. CPT parameters) for offshore windfarm site characterization is given in Siemann et al. (2024).

In addition to the different prediction methodologies, several levels of data integration have been tested to derive these geotechnical values. Studies by e.g. Goodman et al. (2021) and Sauvin et al. (2022b) have applied geostatistical methods only using the geotechnical parameters as input for offshore wind farm site investigation data, together with the interpretation as structural constraint. This works reliably, when having closely spaced geotechnical locations available (e.g. after the main geotechnical campaign is performed) if the geology is not complex and the locations are close to each other but becomes challenging when data is sparse (e.g. during desktop studies or in pre-investigation phase). This is why recent studies tend to incorporate seismic data as guided information in the prediction process. Only few studies have incorporated seismic data within a geostatistical framework (Sauvin et al., 2019; Vanneste et al., 2022; Siemann et al., 2024). In ML, commonly seismic data is directly used in the training of data, with exceptions e.g. in Shoukat et al. (2023). Many data-driven studies are available which include either a handful of selected post-stack seismic attributes (e.g. Vardy et al., 2018; Carpentier et al., 2021; Chen et al., 2021; Sauvin et al., 2022a; Atkins et al., 2023; Qu, 2023) or direct extraction of information from seismic data (e.g. Beyer et al., 2023; Di et al., 2023) in the prediction process. More recently pre-stack seismic inversion is getting increasing attention to derive elastic soil parameters from the seismic data (Karkov et al., 2022; Horn et al., 2023; Cox et al., 2024; Dalgaard et al., 2024). In any case, prediction is either performed in 3D space, which is connected to higher uncertainty if no 3D seismic data is available or along 2D seismic lines, commonly at seismic trace locations. However, most studies do not aim to investigate the application of the predicted geotechnical parameters in the design process of offshore support structures, except recent studies, e.g. by Sauvin et al. (2019), Charles et al. (2022), Zhao et al. (2024) and Arnold et al. (2019).

A reason for this lies, amongst others, in the requirement that current standards such as the German BSH (2014), Eurocode 7-2 (DIN EN, 1997-2, 2010) and DIN 4020 (2010) have to be fulfilled, which require a minimum of one investigation per foundation. Therefore, there was no need to incorporate an interpolated soil profile including the associated uncertainty. However, considerations for including other sources of uncertainty in the design of piles on- and offshore have been conducted and will be implemented in the second generation of the Eurocodes. The uncertainty usually is accounted for by performing a probabilistic analysis. Experience in the probabilistic design of axially and laterally loaded piles and pile foundations has been documented for example by Tandjiria et al. (2000); Pula, 2007; Huang et al. (2016). Recently, these principles have also been applied to offshore wind turbine foundation structures, specifically monopiles (e.g., Carswell et al., 2015; Damgaard et al., 2015; Depina, 2016; Depina et al., 2015; El Haj et al., 2019), since monopiles being currently the most used foundation type for offshore wind turbines. The findings demonstrate that variability in soil parameters can have a significant impact on soil-monopile interaction and thus on the monopile design.

In the current standard design process, which is hereafter referred to as “deterministic design”, this variability is covered by partial safety factors and the selection of cautious characteristic values for the soil parameters. The derivation of these parameters usually relies on the statistical evaluation of correlated parameters from the conducted CPTs in combination with laboratory tests, often also incorporating engineering judgement.

Uncertainties in the description of the subsurface pose a risk to the offshore foundation structures and design needs to be safe as well as cost efficient. A reduction in pile dimensions can have a significant effect on windfarm development costs. Despite the reduction in costs for pile dimensioning, great interest is noticeable from the industry to reduce site investigation costs and shorten timelines in the early stages of windfarm development by making use of predicted geotechnical parameters. This becomes especially interesting when relocations of wind turbines are necessary due to changes in the windfarm layout, but the geotechnical campaigns have been already performed on the originally planned locations. Per regulation, the developer would need to acquire new data at the new location which increases development prices and causes delays due to the execution costly geotechnical campaigns, which normally cannot be performed on short notice due to the high demand of specialized vessels. It is challenging to apply predicted data in real cases, since they need to proof their applicability and need to be accepted by the certification bodies. There are however a few examples where predicted data was and is used in a certified design. A tendency is going in the direction to include those results in the decision making in offshore wind farm development by authorities like Rijksdienst voor Ondernemend Nederland (RVO, Netherlands Enterprise Agency) (e.g. Forsberg et al., 2022) and Bundesamt für Seeschifffahrt und Hydrographie (BSH, public institution for maritime tasks in Germany) but also increasingly by developers themselves. For a better acceptance of the predicted data, studies also incorporating the effect of uncertainty in spatial interpolation are needed.

This study aims to (a) investigate the use of predicted geotechnical parameters including their uncertainties derived from pCPT profiles and (b) assess their applicability on the design process of monopile foundations, mainly in an early phase, in a reliability-based (probabilistic) as well as a deterministic design framework. The use of pCPT profiles has the potential to reduce windfarm development costs. Thereby, the deviation from predicted to real measured data on the design process is analyzed to assess if the predicted data can be used equivalently and safely in the design process. For this case study, site investigation data from a developed windfarm area from the German North Sea is used.

Prediction of the pCPT is done using geostatistical co-simulation (turning bands simulation or TBS), focusing on predicting the corrected cone resistance (q_t) and sleeve friction (f_s) of a fictious CPT at any chosen unexplored location. From the seismic data, acoustic impedance (Z_p) is inverted and used as guided variable for the co-simulation. Geostatistical simulation has been widely used in mineral resources estimation and classification (Verly and Parker, 2021; Silva and Boisvert, 2014), reservoir characterization (Pyrcz and Deutsch, 2014; Peignard et al., 2024), and geotechnical modelling (Masoudi et al., 2024, 2025). Siemann et al. (2022, 2024) have applied it in offshore wind subsurface investigation.

The predicted geotechnical data, i.e. the CPT parameters and based on those derived values for leading design parameters as the effective friction angle, is afterwards used for determining the design length of a lateral loaded monopile foundation. The soil parameters are only derived from the pCPTs using a transformation model from the literature and no laboratory data is included. The uncertainty associated with the used transformation model is not accounted for in the analysis to focus on the spatial uncertainty. Different approaches are assessed and compared to provide a link of deterministic and reliability-based formulations for the evaluation and use of pCPTs showing that comparable results can be derived.

2. Study area and data

The data used in this case study is representative for the conditions in the German North Sea. With water depth ranging from approximately 20-25 m and favorable geological conditions, the site allows for the installation of monopiles.

2.1. Geology

Geologically, the shallow subsurface of the study area is very much influenced by the last ice ages. Overriding ice sheets and sea level changes played a major role in the development of the area, controlling erosion and sedimentation processes during the Pleistocene (Lohrberg et al., 2022b). The site underwent several glacial periods, while being covered by ice sheets during the Elsterian (400.000 to 320.000 years ago) and Saalian (310.000 to 126.000 years ago). Throughout the Weichselian (115.000 to 11.600 years ago), ice sheets have not reached the investigation area (Winsemann et al., 2020; Lohrberg et al., 2022a).

The repeated climate and sea level fluctuations during Pleistocene increased the sedimentation in the North Sea. During glacial periods moraine deposits occurred. Beneath the ice sheets deep tunnel valleys developed which were filled in again by sediments e.g. meltwater sands. In the following inter-glacials, the North Sea region experienced glacier melting and transgression, leading to tidal flat and brackish water sediment deposits besides marine deposits, partly with till layers developing. The Pleistocene deposits are overlain by Holocene sediments, predominantly of marine and terrestrial origin. Outflowing meltwater streams incised channel systems which were subsequently filled with heterogeneous sediment again. In addition to glacial deposits, marine sediments such as basin clays, silts or fine sands, fluvioglacial sediments as well as limnic and brackish sediments can be found in accordance with the aforementioned facies changes.

The Holocene and Pleistocene sedimentary deposits are mainly consisting of fine to medium sands with in situ relative densities ranging from very loose to very dense. The few meters thick Holocene sand top layer is partly underlain by weak layers (e.g. loose sand, clay). Below it follow Pleistocene sands intercalated with varying thicknesses of silt, clay and till layers.

2.2. Geophysical and geotechnical data

A comprehensive geophysical survey was conducted in the investigation area including a 2D ultra-high-resolution (UHR) seismic data acquisition together with a detailed geotechnical campaign with CPTs and boreholes. The 2D UHR data was collected during research cruise He569 in 2021. The 2D-multichannel seismic data has been acquired using a two-chamber mini GI-Gun source and a 96 channel streamer with different hydrophone spacings, having a total active length of 228 m. For a detailed description of the acquisition set-up the reader is referred to the cruise report (Keil et al., 2021).

For this study a 2D UHR seismic profile (He569-GeoB21-033) is being used in combination with a total of 8 CPT profiles along the seismic line (Fig. 1). Penetration depths of the CPTs range from 45 m to 60 m below seabed. The maximum offset from the seismic line is ~170 m. The offset between the CPT and seismic line can cause potential mismatches between the CPT data and the seismic data which introduces uncertainty in the prediction and modeling process. Offsets can lead to vertical shifts between the data or the presence or absence of deposits due to a heterogeneous subsurface. The general distances between the CPTs range from 1012 m to 1922 m. The CPT cluster to the east of the profile contains several CPTs with only short distances of up to 20 m from each other. The CPTs have been migrated onto the seismic line and are adjusted for depth and horizontal position. The CPT data is a

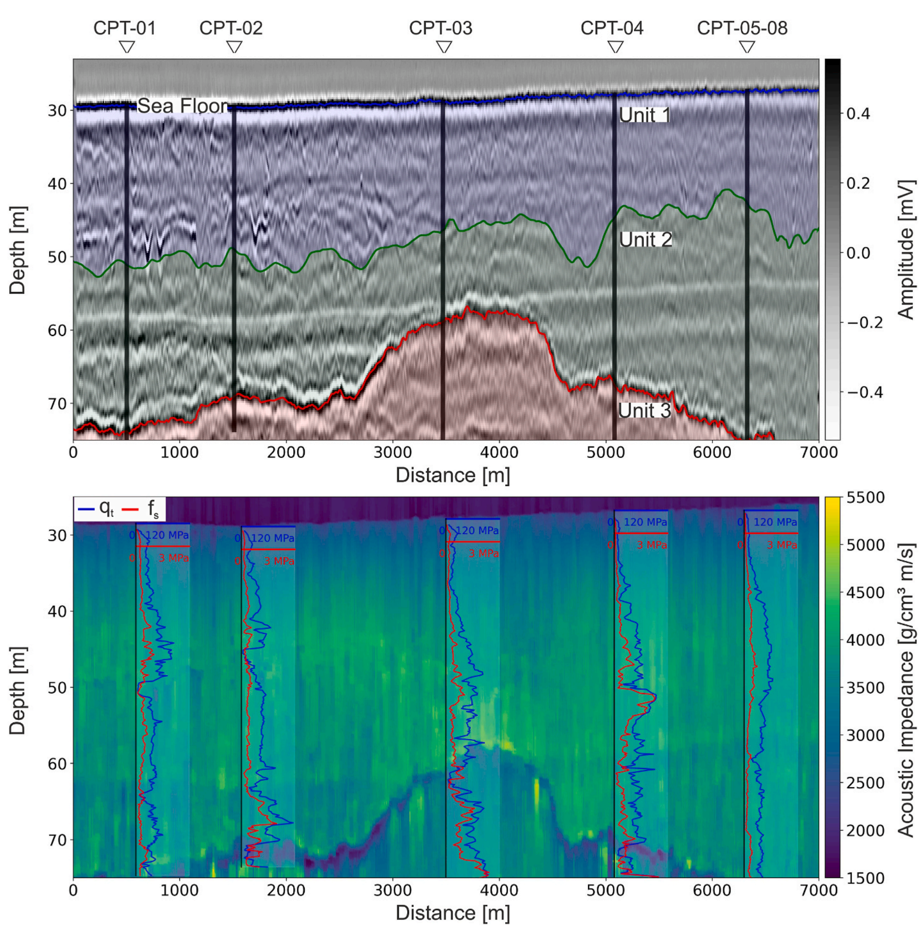

Fig. 1. Illustration of the input data being used in the prediction process. Above: 2D seismic reflection data showing the interpretation on the line. Below: Acoustic Impedance, together with the CPT log curves for q_t (blue curves) and f_s (red curves). (For interpretation of the references to color in this figure legend, the reader is referred to the Web version of this article.)

set of downhole CPTs, which were cleaned from outliers being caused by the operation procedure before being used in the prediction process. The data gaps were not filled to avoid including artificial data in the further process. The process is performed in depth domain.

Absolute acoustic impedance is used as co-variable to guide geotechnical parameter prediction. The band-limited acoustic impedance was generated from the post-stack seismic data and merged with a low-frequency model based on interval velocities. A more detailed description of the inversion process is given in Siemann et al. (2024). Generally, the acoustic impedance increases with depth while obtaining a low impedance layer at the layer boundary of unit II and unit III, which corresponds to clay deposits as indicated by the CPT and borehole information.

Marine sediment acoustic response is governed by sediment structure, dynamic strain amplitude, overburden stress, lithification, and grain size (Stoll, 1989), which also influence cone resistance and sleeve friction measured by CPT (Vardy et al., 2018). However, P-wave seismic attributes such as velocity and acoustic impedance are acquired at very small strains, whereas CPT parameters reflect large-strain penetration and shearing, so the methods probe different portions of the constitutive response (Vardy et al., 2018; Sauvin et al., 2019). Empirical and physics-guided correlations linking dynamic (small-strain) stiffness to large-strain, static properties and construction parameters are well established, particularly for normally consolidated, uncemented soils (e.g. Wichtmann et al., 2017). These relationships become more complex in brittle or cemented materials and in sediments with significant stress-history effects (e.g., glacial loading) and variable depositional histories, where bonding, anisotropy, and fabric modify both seismic and CPT responses (e.g. Vardy et al., 2017). However, it was shown that acoustic impedance and cone resistance exhibit a positive, nonlinear correlation (Opeyemi, thesis; Vardy et al., 2018). Therefore, both parameters have been jointly used to predict geotechnical parameters and develop ground models in several studies (Carpentier et al., 2021; Beyer et al., 2023; Qu, 2023).

3. Methodology

3.1. Prediction of CPTs using geostatistical co-simulation

A CPT prediction is performed to compute the statistics of the geotechnical properties at each location along the 2D profile. The target parameters for the CPT prediction are the corrected cone resistance (q_t) and sleeve friction (f_s). Acoustic impedance (Z_p) is used as guided variable for the prediction process. The general simplified modeling workflow is shown in Fig. 2. A detailed description follows in the subsequent sections.

3.1.1. Geostatistical simulation background

Kriging is a linear geostatistical method which uses local weighted averaging of surrounding measurements to obtain spatially interpolated information at the desired point. The term "linear" means, that the interpolated value is a linear combination of measured data considering kriging weights. Kriging weights depend mainly on the location and configuration of surrounding measurements, as well as the model of spatial variability, i.e. using a variogram for a univariate and cross-variogram for a multivariate dataset. The linear kriging method provides an unbiased estimate, i.e. the error expectation is zero, as well as a minimized error-variance of the estimate and therefore provides a quality measure of the interpolation. Co-kriging methods have been developed to model multivariate datasets. The advantage lies in reproducing linear correlation between the input variables in the interpolated values (Wackernagel, 2003). In addition, an auxiliary variable with better geographical coverage may improve the model of the principal variable. However, linear interpolations (kriging, co-kriging and other variants) possess two drawbacks (smoothing effect) which make them insufficient for real risk assessment problems:

- The kriging method produces a rather smooth solution, which on average overestimates the low values and underestimates the high values, especially if the distance between the measurements is too high (compared to the variogram range).
- It does not retain the spatial variability of the input data and corresponding uncertainties. In other words, the variogram of the output model is inferior to the variogram of the input measurements.

To overcome these disadvantages, geostatistical simulation methods have been developed. In mineral resource estimation and classification (e.g. Journel and Huijbregts, 1981) and reservoir characterization (e.g. Pyrcz and Deutsch, 2014), these methods have a long history of application, whereas there are only few recent case studies in geotechnical applications (e.g. Masoudi et al., 2023, 2025) or in the offshore wind-farm development (e.g. Siemann et al., 2022, 2024). Geostatistical stochastic simulation could be imagined as a spatial Monte Carlo model which is meant to honor the spatial variability of the measured data, reproduce the input data histogram and assess the uncertainty in the predicted model (Chambers et al., 2000). It can replicate, for instance, a multimodal distribution with pronounced tails in comparison to the kriging result. For details on the methodology see for example Chiles and Delfiner (2012) and Pyrcz and Deutsch (2014).

The interpolation methods such as kriging only predict one value

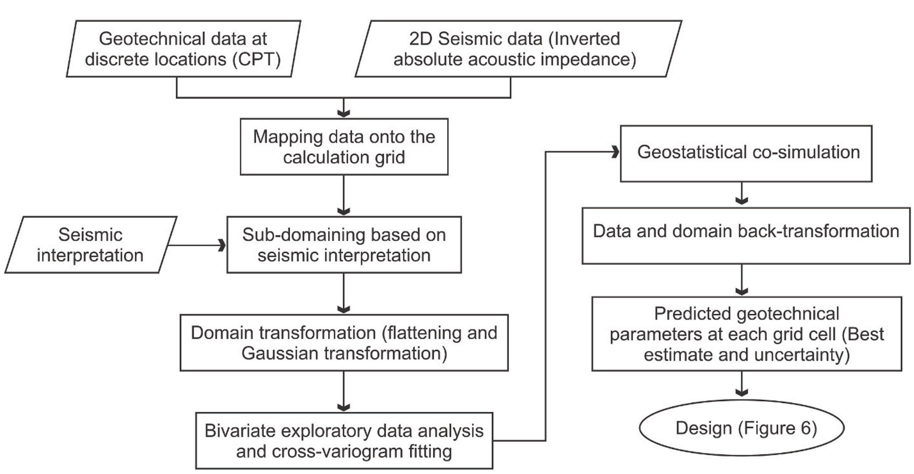

Fig. 2. Process workflow of the methodology applied in this study, to derive geotechnical parameters at unexplored positions using geostatistical simulation and its use for probabilistic foundation design.

(the most expected) at every point of interest. Geostatistical simulation returns equally probable solutions (scenarios or realizations), honoring the statistical moments (mean and variance) of the input data set. Therefore, for each point of interest a probability density function (PDF) can be computed. Fig. 3 shows this concept schematically for a 1D CPT cone resistance profile located in a 2D cross-section of q_t-predictions. This can be used for uncertainty and probability analysis, therefore risk assessment and decision making. At each point of interest, the mean of all the realizations is close to the kriging prediction.

There are three well-known geostatistical simulation methods for probabilistic modelling of a continuous variable: sequential gaussian simulation (SGS), turning bands simulation (TBS) and stochastic partial differential equations (SPDE). Between the classical simulation based approaches (SGS and TBS), the TBS is a computationally more efficient algorithm however, impractical in case of having locally varying anisotropies within folded strata due to straight bands generated during unconditional simulation. The SGS has been developed based on simple kriging, which considers strict stationarity (Chiles and Delfiner, 2012). The SPDE is a more recent development, showing good performance in calculation speed and managing local anisotropies, it is mostly used in two-dimensional mapping at regionalized scale (Lindgren et al., 2011; Fuglstad et al., 2015). In case of the problem investigated in this paper the TBS is chosen due to its high computational performance and efficiency with large amount of data as well as more tolerance regarding the stationarity hypothesis. The TBS-algorithm, which was originally proposed by Matheron (1973), consists of a two step approach (Chiles and Delfiner, 2012), which is repeated to generate 10 000 scenarios or realizations:

- Unconditional simulation: drawing random bands in space (here 10 000 bands are used) (Fig. 4). On the bands, generating a random gaussian variable, respecting the variogram model. Combining projections of the gaussian random values to the location of inputs and outputs.
- Conditional simulation: at the location of inputs, calculate the residuals by subtracting the unconditional simulation from the input data (gaussian transformed). Applying ordinary kriging to the residuals to generate the interpolation of residuals on the outputs. Finally, summing interpolated residual with the unconditional simulation, and back-transformation from the gaussian distribution to model the geotechnical parameters.

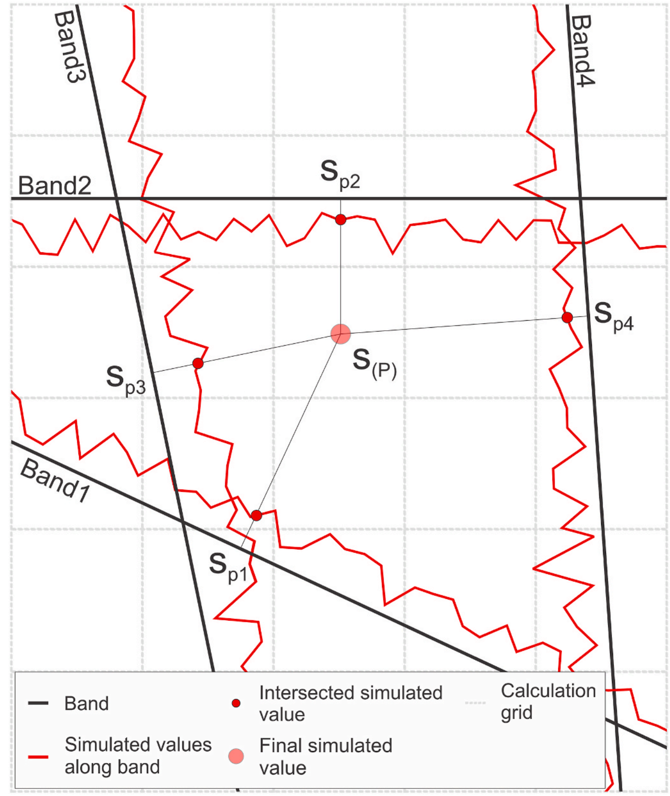

Fig. 4. Schematic representation of the unconditional simulation TBS procedure used to compute a simulated value at location S(p). For the grid cell centered at S(p), perpendiculars intersect the bands at Sp_1–Sp_4, from which the simulated values are extracted (red dots). The final simulated value at S(p) (light red circle) is computed as the normalized average of these four contributions. This is the representation of first step in the TBS procedure, which is followed by the conditional simulation. (For interpretation of the references to color in this figure legend, the reader is referred to the Web version of this article.)

3.1.2. Space deformation and geostatistical modeling

The geostatistical modeling workflow is performed in the commercial software Isatis.neo™ (2024). After data import, a calculation grid is created covering the extent of the 2D seismic line. The resolution is 0.1

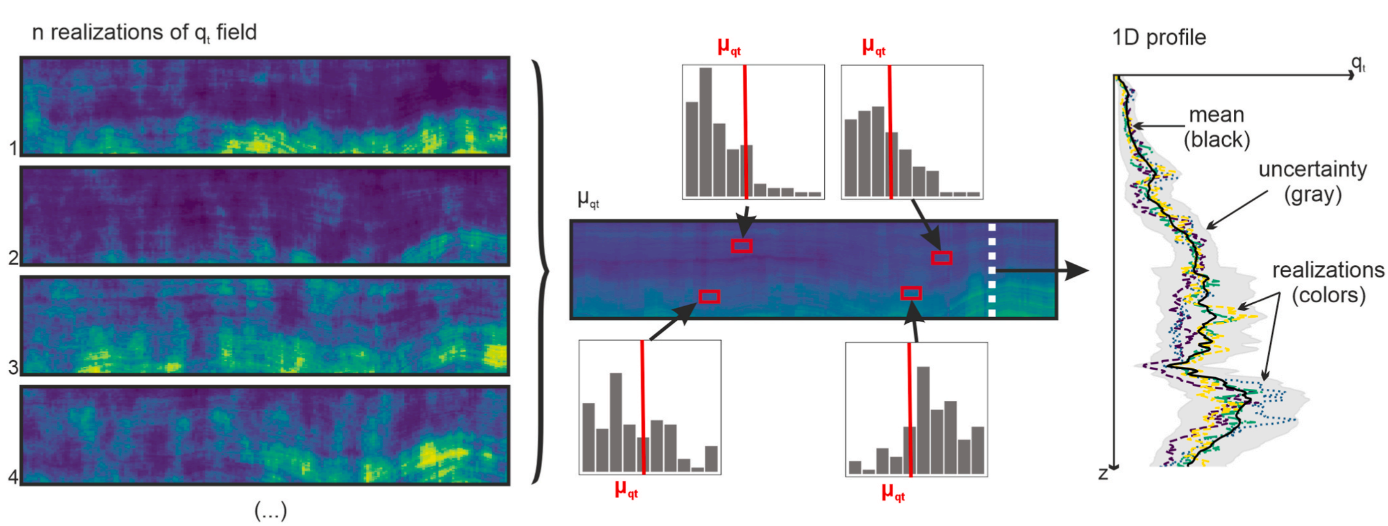

Fig. 3. Conceptual figure showing different equally possible realizations on a prediction grid for the predicted cone resistance. The average of the different outcomes is considered as the best estimate. Each Grid cell has an individual output distribution based on the simulated values. At each point of the model, vertical predicted 1D profiles can be extracted containing information about the mean prediction as well as its uncertainty and the individual realization results.

m in vertical and 10 m in horizontal direction, with the midpoint of the individual grid points corresponding to a seismic trace value. The seismic data and CPT parameters are mapped onto the grid. To match the vertical resolution of the different data inputs, the CPT data is upscaled using the moving average technique from 2 cm vertical measurement interval to the resolution of the geophysical data. The grid is transformed into flattened space prior to geostatistical modeling.

Sedimentary deposits that have been affected by tectonic activity or dynamic sedimentary systems, such as river channels or tunnel valleys, can result in a high variability within the deposits, thereby decreasing the spatial continuity of geotechnical properties. To improve spatial continuity, geostatistical modeling is carried out in a "flattened space" through coordinate transformation in the vertical direction (Fig. 5). A technique known as "unfolding" is used to address geometrical heterogeneities by either restoring sedimentary layers to their original state before tectonic deformation or erosion, or by adjusting for non-horizontal, varied layering (Caixeta and Costa, 2021; Chautru et al., 2021; Chautru, 2024). Interpolation of geotechnical parameters and seismic measurements in flattened space allows for the horizontal alignment of measurements, which correspond to an individual geologic layer. The applicability of this method was demonstrated by Wu (2017) using borehole data and seismic data. The application of flattening becomes more advantageous in the geotechnical characterization of a thin strata (Masoudi et al., 2024). Modelling in flattened space is well applicable in this geological setting where deposits are quite continuous. However, care needs to be taken in more challenging environments where complex erosional events (e.g. tunnel valleys) are present or in tectonically complex regions.

From the interpreted horizons shown in Fig. 1, three key horizons were identified and applied to the flattening, each done separately across three intervals based on the seismic interpretation. The geostatistical steps were conducted individually for each of the three units, i.e. to account for both geological variations and geotechnical interpretation.

The gaussian transformation is applied to the geotechnical parameters and is further used for variographical analysis. After the modeling of the cross-variograms, co-simulation is performed to generate 10 000 realizations within each unit. The resulting gaussian PDF for each target point is then back-transformed to generate PDF of geotechnical parameters, e.g. the CPT-tip resistance q_t (s Fig. 3). In the last step, the coordinates are back-transformed from the virtual flattened space into the real space for further analyses (compare Figs. 2 and 5).

3.1.3. Spatial variability (variogram) and neighborhood selection

In geostatistics, the variogram is a characteristic of a regionalized variable (here the geotechnical parameters), based on which kriging and simulation weights are attributed based on the location relative to the surrounding samples. It is a measure of spatial variability, defined as a function of Euclidean distance (e.g. Gringarten and Deutsch, 2001; Masoudi, 2022). The Variographical analysis is the process of plotting an experimental variogram based on the available measurements then fitting an ascending mathematical function, called variogram model. On a stationary regionalized variable, a basic variogram model is defined by:

- nugget effect: inferior bound of variogram model, which is the variability at distances close to zero.
- sill: superior bound of variogram model, which is the maximum variability of the regionalized variable, comparable to the statistical variance.
- range: the Euclidean distance at which the variogram model reaches its sill, which is the maximum distance of spatial correlation.

Since geostatistical co-simulation is performed in this study, a directional cross-variogram, consisting of three variogram plots (same structures and same ranges) need to be fitted (sill matrix) for each unit. Two simple variograms for the spatial continuity of the main (q_t or f_s) and auxiliary or guided (Z_p) variables and a cross-variogram between them were modelled to consider conjointly the spatial behavior. The Supplementary Material Figs. S1–S3 shows the directional variogram models used for each unit. In Tables S1–S3 the parameters for the chosen variograms are listed. As for the search neighborhood the vertical and horizontal direction are considered separately. Due to the deposition process, the spatial continuity in the horizontal direction is larger compared to the vertical direction, describing the anisotropic nature of the subsoil.

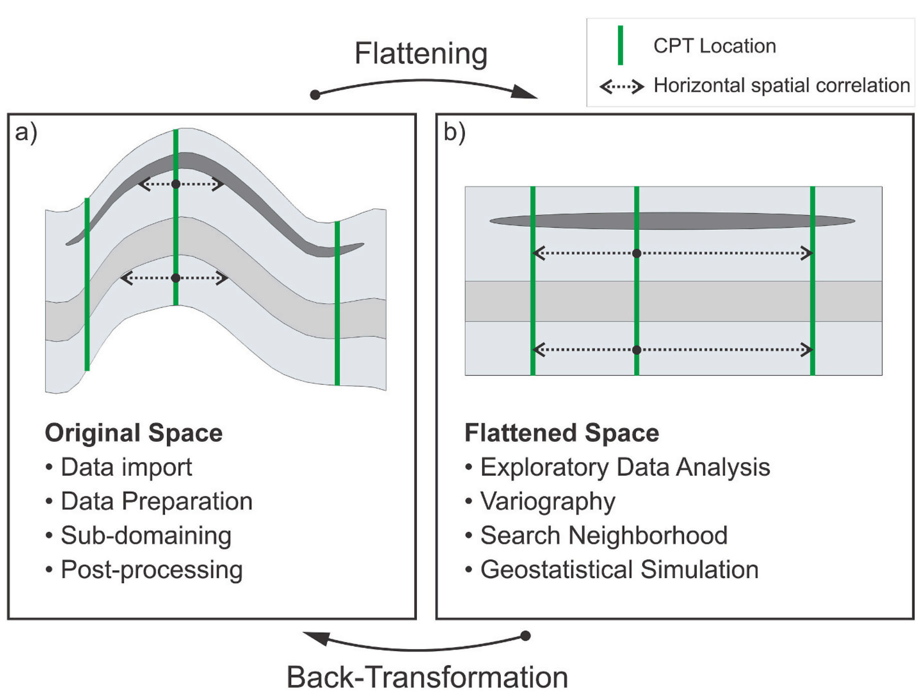

Fig. 5. Sketch showing the space deformation by unfolding for improving horizontal spatial correlation. The different key steps in each space are listed below.

The variogram fitting procedure includes subjective uncertainty. It has been fitted best based on the data, the knowledge of the local geology, the data quality and accounting for outliers. Variogram parameters are shown in the supplementary material Table S1 to Table S3 The nugget effect for all variograms is set to be zero, assuming no spatial variability at zero distance. The local geology obtains very homogenous deposits leading to the assumption that long horizontal continuity is expected. That, together with improving spatial continuity using the flattened space results in very long ranges in the horizontal direction. Therefore, lower variability is assumed even at long horizontal distances, whereas the variability remains high in the vertical direction. The low variability in the horizontal direction covers the far distances between the CPT boreholes. Since vertically, a lot more data points are available along the boreholes, the variogram modeling is more objective and straightforward, even if more spatial variability is observed. To improve variography in horizontal direction it is recommended to have more CPTs distributed over the area or CPT clusters. Both would increase the confidence of variographical analyses while the latter would specifically address the short distances.

In vertical direction, shorter ranges of a couple of meters are encountered, introducing higher variability on shorter distances, which is expected due to the stratification. Therefore, the neighborhood radius is chosen to be higher laterally (higher spatial continuity and less data frequency) than along the vertical direction. Vertically, the neighborhood radius is selected to be 2.5 m. Horizontally, 3000 m has been chosen to ensure several CPTs are considered to predict a target point and to ensure full coverage along the line. The weighting of the selected data points within this search neighborhood is defined by the variogram model. The number of bands was chosen to be 10 000 and 10 000 realizations (scenarios) were generated to assure the representativity of the probabilistic modelling. Table 1 shows an overview of the parameters being defined for the simulation. The settings are kept constant for the different geological units.

3.1.4. Prediction quality control

For the assessment of the prediction quality, each measured CPT is systematically removed from the prediction. The prediction results are then compared at this CPT location with the real measured data (leave-one-out/blind testing). Due to their proximity to each other, the CPT cluster to the East of the seismic profile is removed as one. Removing a CPT leads to a large gap between the locations (between approximately 2700 m and 3500 m). That implies that for each point to be predicted a distance to measured geotechnical parameters from CPT is always more than 1000 m. Within those large distances, a lot of geological changes might occur, which may not be replicated perfect by the modelling process. Also, the large distances show the need to incorporate secondary information like seismic data to guide the prediction process. The prediction does not rely heavily on the auxiliary data since the sum of weights of the auxiliary variable is zero, i.e. the order of magnitude of auxiliary variable is neutralized. However, the sum of weights of the principal variable is one honoring the universality condition to guarantee an unbiased estimation. The information is inferred from the relationship between the acoustic impedance and CPT parameters through the cross-variogram.

Consequently, five predictions are performed for each parameter of interest to allow quality control at each CPT location by plotting and comparing the measured and predicted results. The variogram model is kept the same throughout the calculations and is not adjusted for each new data set which is created when removing a different profile. Keeping the variogram model constant is justifiable since the aim is investigate the impact of estimation in the cross-validation and not the influence of variogram changes. Direct comparison of measured and predicted results is useful in assessing local and overall differences. The uncertainty of the prediction is considered in the form of three times standard deviation in the illustrated predicted profiles (see chapter 4.1, Fig. 9). Three times standard deviation was chosen following the three sigma rule (Grafarend et al., 2022), showing the interval, in which around 99.7 % of the values would lie within a normal distribution. The authors believe this representation of uncertainty is more intuitive than one showing only one standard deviation (sigma), as it highlights potential local minima and maxima for engineers. However, 68.3 % of the probability mass is already lying in the interval of ± one sigma.

In order to judge the quality of the estimation, specifically along the 2D seismic line section, the coefficient of variation (CV) is calculated as followed: $CV = \sigma_{pred} / \mu_{pred}$, with μ_{pred} being the mean or best estimate of the prediction at the target location and σ_{pred} its standard deviation. The CV is a normalized measure of dispersion around the mean, which allows for the direct comparison of the prediction quality of q_t and f_s. Where CV is low, less uncertainty is encountered, while with higher C V also the uncertainty increases due to higher scatter of the standard deviation in relation to the mean (see later Fig. 9).

Table 1
Model parameters for the TBS performed in this study.

Vertical search neighborhood	2.5 m
Horizontal search neighborhood	3000 m
Number of bands	10 000
Number of realizations	10 000

3.2. Design process for a horizontally loaded monopile

The pCPT profiles are further used for the geotechnical design of monopile foundations, in which the design length is estimated using a displacement criterium of the pile head as it is done in preliminary design, i.e. for cost evaluation. Hereafter the concept of a reliability-based design framework, is briefly outlined. This is followed by the design assumptions made for this study.

3.2.1. Reliability

The designer is responsible to ensure a safe and reliable design of the structure. Reliability hereby means that the structure will perform its intended function without failure with respect to a given target reliability for the envisaged design lifetime. Guidelines for this design task are defined in standards, which specify, for example, values for material properties, loads, and verification methods. In Europe a common framework, i.e. the Eurocodes (EC), was established, on which the national standards are built.

According to Eurocode 0 (DIN EN 1990; 2021) every structural verification is based on the formulation of limit states. A limit state is a condition beyond which a structure or structural element no longer fulfills its intended function, usually defined by a single failure mechanism, i.e. the structure becomes unsafe or unusable (DIN EN 1990; 2021). Design usually is differentiated between ultimate limit states (ULS), where strength or stability problems occur, fatigue limit states (FLS) and serviceability limit states (SLS), where deflection, vibration or other features are not tolerable. Regardless of the limit state type, usually actions (loads, temperature, etc.) F and resistances R are compared. Generally, a response function $G(\boldsymbol{X})$ is mathematically formulated for which the limit state can be defined as

$$G(\boldsymbol{X}) = G(X_1, X_2, \ldots X_n) = 0 = \frac{F(\boldsymbol{X})}{R(\boldsymbol{X})} \text{ or } F(\boldsymbol{X}) - R(\boldsymbol{X}) \tag{1}$$

with $F(\boldsymbol{X})$ and R $(\boldsymbol{X})$ being exemplary the loads and resistances respectively.

The limit state function defines the boundary between the safety domain $G(\boldsymbol{X}) > 0$ and the failure domain $G(\boldsymbol{X}) \leq 0$ for a given structure (Lemaire et al., 2009). $\boldsymbol{X}$ are (random) variables representing the uncertainties in action and resistance, which are based on experiences and measurements regarding material parameters, or loads (Melchers, 1999). In the case of this study $\boldsymbol{X} = f(q_t, f_s)$ with q_t and f_s being modelled based on the uncertainty computed using the developed algorithm (s Fig. 10).

The probability that a structure fails therefore is

$$p_f = \Phi(-\beta) = P(G(\boldsymbol{X}) \leq 0) \quad (2)$$

with β being the reliability index and $\Phi(\cdot)$ being the cumulative probability density of the standard normal distribution. The reliability of the structure is the probability of failure not occurring.

EC 0 provides target reliability indices for different limit states and reference periods. For a SLS and a reference period of one year, the target reliability is given with $\beta_t = 2.9$, resulting in a target probability of failure not to be exceeded of $p_{f,t} = \Phi(-2.9) = 1.9 \cdot 10^{-3}$ (DIN EN 1990; 2021). To ensure the same reliability level for a 50 year reference period the target probability of failure is $p_{f,t} = \Phi(-1.5) = 6.7 \cdot 10^{-2}$ (Vrouwenvelder et al., 2024).

Instead of using these fully probabilistic approaches, the Eurocodes established a so-called semi-probabilistic design concept, in which the uncertainties on loads and resistances are modelled using characteristic values in combination with partial safety factors. The characteristic value is a deterministic estimate of, e.g. strength or load properties, accounting for all uncertainties associated with the derivation of this value (variability, sample size, sample quality, experience, etc.). According to DIN EN 1990 (2021), the characteristic value is typically defined using the 5% fractile as a lower critical bound and the 95% fractile for an upper critical bound. This approach can be interpreted as deterministic approach, as the uncertainties are implicitly accounted for, but the resulting deformation or factor of safety does not explicitly provide an answer on how likely the outcome is. On the other hand, applying a reliability-based approach, the full probability (function), i.e. the uncertainty, in the properties is used explicitly and thus results in the computation of the probability density function of the response function $G(\boldsymbol{X})$ from which the reliability can be readily computed.

3.2.2. Geotechnical analysis model

3.2.2.1. Definition of the limit state. The design length of a monopile is often determined by a displacement criterion, in order to ensure the foundation's stable behavior, even under cyclic loading. This criterium is mostly defined with respect to the lateral deflection or rotation of the pile head, as the mechanical components of the wind turbine (generator, gearbox, etc.) define the allowable tilt of the monopile head (Savidis et al., 2018). Different limit state formulations for this evaluation have been established in recent years. For the here presented example the corresponding limit state function $G(\boldsymbol{X})$ is chosen as

$$G(\boldsymbol{X}) = 1.1 \cdot \delta(\boldsymbol{X}, L = 60 \text{ m}) - \delta(\boldsymbol{X}, L) \quad (3)$$

where δ is the lateral head displacement, L is the pile length (pile tip to seabed) and $\boldsymbol{X}$ is the random variable representing the variability of the soil property values in the pCPT profile. Hereby, the variability is the spatial variability due to the interpolation. The criterium refers to: If the head displacement for a specified pile length is more than 1.1 times larger than for a theoretically infinite pile, approximated by a calculation for $L = 60$ m, the limit state function takes a value of $G(\boldsymbol{X}) < 0$, which implies serviceability failure. This criterium has been used in several projects especially in the preliminary phase, in order to get an estimate of the necessary pile length, which shows stable behavior also under cyclic loading. It has turned out that a certain amount of conservatism is included in the pile length derived by this criterion, so a number of other comparable deformation criteria has been used in design, e.g. other percentage values or the ratio between pile head and pile tip rotation. The process described hereafter is not affected by the criterium itself, so it can be readily applied to account for any other limit state.

Nevertheless, additional criteria have to be applied in practice (e.g. ULS for pile end bearing in use and during installation).

While the soil properties are taken as probabilistic or deterministic dependent on the calculation approach (see the following paragraphs), the loads in this analysis are considered as deterministic. Nevertheless, a full probabilistic approach can also account for the stochastic nature of loads (Zorzi et al., 2020).

3.2.2.2. Calculation principles and design assumptions. The pile deformation of a laterally loaded pile can be determined, amongst other models, by using a model of an embedded beam, where non-linear springs account for the soil-pile interaction, with the spring stiffness depending on the soil properties and depth. The springs are modelled as so-called p-y-curves based on ISO 19901-4:2025 (formerly "API-Standard") with some adaptations for different effects such as large diameters or small strains described e.g. in Arnold et al. (2019, 2022). The formulation of the p-y-curves differs for different soil types and is briefly discussed in the following part. Due to the non-linear behavior, the pile response is computed using the finite-element-program RFEM 6© (2022).

The pile is modelled as a 1D-system below the seabed level. Due to the lever arm from the turbine to the seabed the lateral load consists of a bending moment M_k and a horizontal force H_k (Fig. 6). It is common practice to decouple the lateral analysis from the vertical loading mainly coming from gravity forces. Loads of $M_k = 400$ MNm and $H_k = 9$ MN are applied, which are in the range of loads occurring in the German North and Baltic Sea (Lesny, 2008). The loads given by Lesny (2008) represent quasi-static equivalent loads based on a governing extreme event, which are often a decisive case for foundation design. Cyclic load effects have to be accounted for in a second design step, which is not part of this paper. The monopile is assumed as an open-ended steel pipe (Young's modulus $E = 2.1 \cdot 10^5$ MN/m^2) with an outer diameter of $D = 6.5$ m and a wall thickness of $d = 75$ mm. Therefore, the bending moment of inertia is $I = 7.8$ m^4. The lateral springs are set every $a = 0.5$ m with depth, representing the continuous lateral bedding of the pile. The geotechnical analysis model is sketched and summarized in Fig. 6.

3.2.2.3. Derivation of soil parameters and p-y-curves. The construction of the p-y-curves after ISO 19901-4:2025 differs for different soil types. It distinguishes between non-cohesive material (sand) and cohesive material (stiff and soft clay). The explicit formulation can be found in ISO 19901-4:2025.

Generally, the curves depend on the depth z below mudline, the effective soil unit weight γ', parameters describing the strength of the soil and empirical coefficients, which also can be determined based on the strength parameters. For non-cohesive soils the governing parameter is the effective friction angle φ'. For cohesive soils the relevant parameters are the undrained shear strength s_u as well as the strain corresponding to one-half of the maximum principal stress difference ε_{50} in a triaxial compression test, which can be estimated e.g. based on Sullivan et al. (1980).

To classify the soil into cohesive and non-cohesive material Robertson's (2009) normalized classification chart was used. Mixed soils were classified as cohesive, if the friction ratio $R_f = 100 \cdot f_s / q_t$ exceeds a value of 2.5 %.

Since mostly sandy soils are present in the study area, the effective soil unit weight was set to 9 kN/m^3, as recommended by DIN 1055 (2010) for loose sands, which matches the relative density of the top layers. The effective friction angle for the non-cohesive sands was calculated after Kulhawy and Mayne (1990) using Equation (4), with q_t as corrected tip resistance, σ'_{vo} as effective overburden pressure and p_a as atmospheric pressure (100 kPa). This correlation is widely used for inferring the strength characteristics for North Sea sand deposits, despite the fact that numerous other correlations exist.

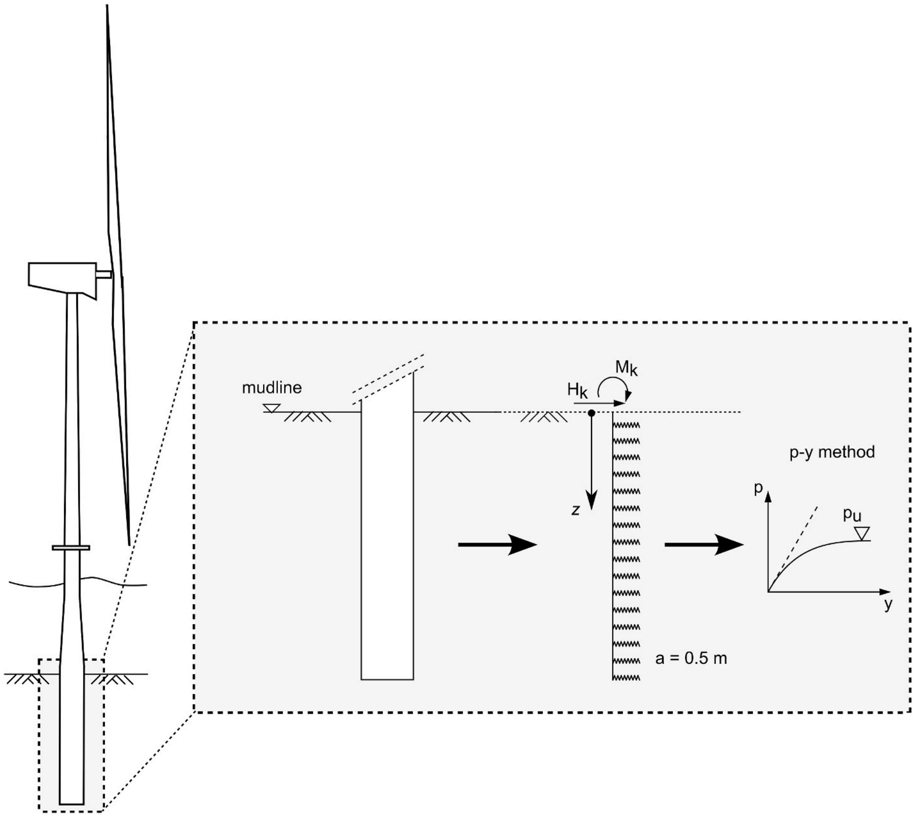

Fig. 6. Geotechnical analysis model for the evaluation of the lateral deformation of a monopile. Not to scale.

$$\varphi' = 17.6^\circ + 11^\circ \cdot \log_{10}\left[\left(\frac{q_t}{p_a}\right) \cdot \left(\frac{p_a}{\sigma'_{vo}}\right)^{0.5}\right] \quad (4)$$

Kulhawy and Mayne (1990) gave a standard deviation of 2.8° for this transformation for the regression analysis. This associated transformation uncertainty was not included in the analysis. Additional information on the transformation uncertainty in the used transformation and others can be found in Ching et al. (2017).

The undrained shear strength for cohesive soils was calculated using Equation (5) after Robertson and Cabal (2022), with σ_{vo} as total overburden pressure and N_{kt} being the cone bearing factor. The factor N_{kt} is usually derived by a comparison of different laboratory tests to measure the undrained shear strength. In this study it is set to 20 for this analysis, which is representative for the North Sea deposits (e.g. Mayne and Peuchen, 2018). s_u was bounded to 200 kPa as maximum value since this is the expected range in the relevant depth for the pile and therefore to avoid unconservative values.

$$s_u = \frac{(q_t - \sigma_{v0})}{N_{kt}} \quad (5)$$

3.2.2.4. Overview of the calculation approaches. For evaluating the pCPTs, the different calculation (design) approaches applied are summarized in Table 2, including the data being used and the output being generated. The calculation schemes are classified as deterministic or reliability-based respectively, as discussed in chapter 3.2.1. For the ease of comparison in this study only q_t is varied, f_s is kept constant in all approaches as best estimate of the pCPT and is only used for classifying the soil type. Yet, this simplification should be handled carefully. For the here presented soil profiles the soil is mainly classified as sand for all ranges of q_t with no change in the type of the p-y-curve. A deviating assignment of the soil type happens only in a depth, where, based on Fig. S4, the authors believe that the change is negligible. However, for other sites for which more cohesive soil or a lot of different layers are present, the uncertainty in assigning the soil unit should be investigated. It could be advisable to fix the soil unit depths in a separate analysis to avoid switching the model formulation. Also keeping R_f constant could lead to a more stable assignment than it is with f_s. Nonetheless, the layer boundaries are still interpolated and even if the geophysical analysis provides guidance some uncertainty is inherent. An additional study should be conducted regarding this topic of combining predicted CPT and layer boundaries. Given the simplification used here, the calculation schemes differ only in their approach of incorporating q_t. The processes of these calculation schemes are described in Fig. 7. For the deterministic approaches either the measured CPT values ("MD") or an evaluation of the probability function of the pCPT ("QD") with its quantile values is used to derive the soil parameters for the p-y-curves. An exemplary graphical representation is shown in Fig. 8. For different pile lengths the lateral pile head displacement is evaluated and an

Table 2
Deterministic and probabilistic calculation approaches used in this study.

Approach	Calculation scheme	Used CPT profile for q_t	Output
MD1	deterministic	measured CPT	specific design length
MD2	deterministic	Design profile by engineering judgement of measured CPT (summing up to thicker layers)	specific design length
QD0	deterministic	Mean of all pCTP-realizations	specific design length
QD *p*	deterministic	Quantiles of the probability distribution of the pCPT: $q_{t,i} = \mu_i \pm p \cdot \sigma_i$ with $p \in +/- \{2, 1.645, 1\}$	specific design length
P	probabilistic	every realization *i* of simulated pCPTs	*CDF* of lengths

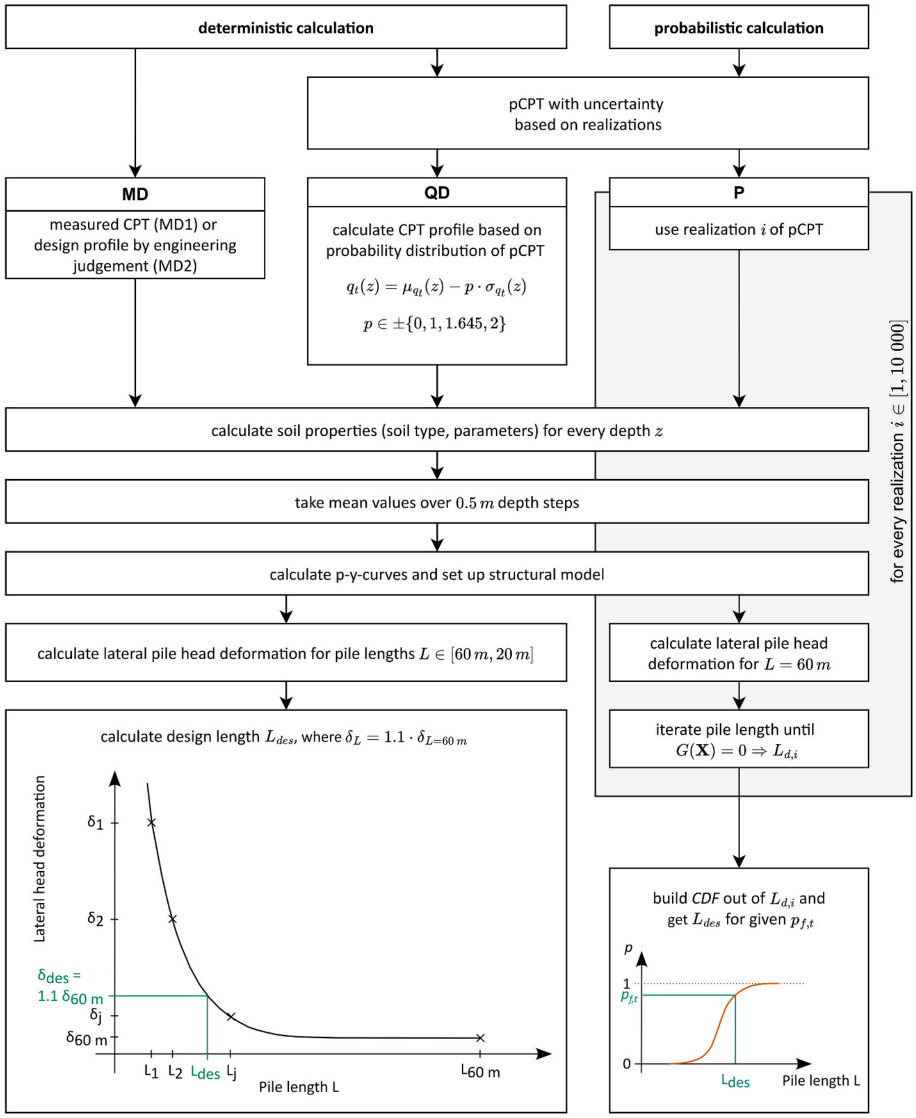

Fig. 7. Flow chart of the workflow for the different calculation approaches listed in Table 2.

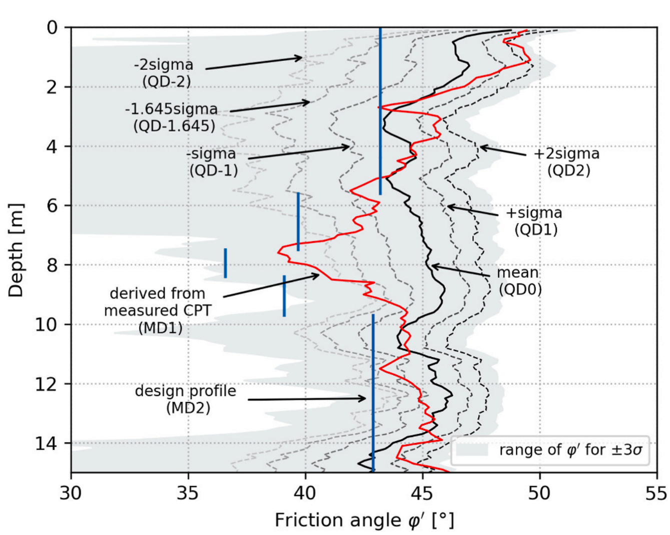

Fig. 8. Exemplary plot for different deterministic approaches after Table 2 for the friction angle. The dashed lines show different factors of the standard deviation, which only partly match the lines in Fig. 8.

approximation curve is constructed. Based on this approximation curve the pile length is determined, for which the limit state function (Equation (3)) is fulfilled. While the deterministic calculations generate one specific deterministic design length L_{des}, the probabilistic approach generates a cumulative distribution function (CDF) of the lengths $L_{d,i}$, where every length presents one of the 10 000 CPT profile realizations (scheme see Fig. 3), for which $G(\boldsymbol{X}) = 0$. For approach P the design pile length is determined in 10 cm steps. The design is determined based on the *CDF* as chosen quantile.

4. Results and discussion

4.1. Prediction of q_t and f_s using geostatistical simulation

Fig. 9 shows the mean m_{q_t} or m_{f_s} of all 10 000 simulations, which is considered as the best estimate for the target parameters q_t and f_s, together with the coefficient of variation CV_{q_t} and CV_{f_s} of the prediction, along the representative seismic line. The application of the space deformation technique as described in section 3.1.2 allows for the predicted parameters to follow the seismic reflectors. The prediction shows a larger variability in the vertical direction compared to a longer continuity (lower variability) horizontal direction. Minima and maxima in the data range match with measured information at known locations.

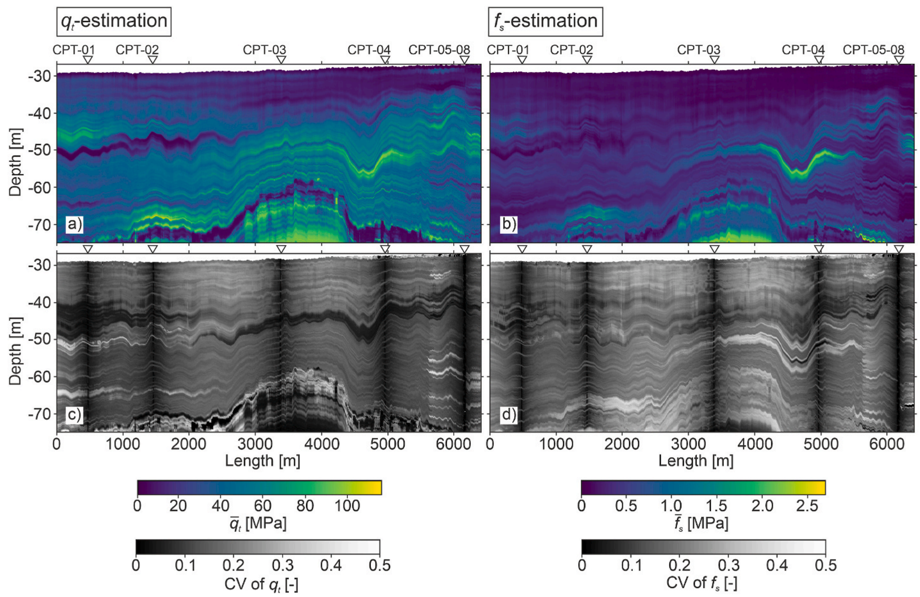

Fig. 9. Prediction of the geotechnical parameters q_t (left) and f_s (right) along the 2D seismic line. (a-b): Best estimate of the prediction. (c-d): Coefficient of variation (CV) of the prediction.

Apart from the CPT profile, local maxima are computed with pronounced features in Z_p. More precise variations in the best estimate are seen in Fig. 10 and described later.

To have a comparable quality of estimation between the different target parameters, the *CV* is used as a standardized measure of variation, making both results directly comparable. In Fig. 9(c and d) the black color indicates a low *CV* and white addresses a high *CV*. *CV* is low at and close to the CPT locations. Where data gaps from cleaning are present in the measured CPT data, higher *CV*- values are observed. For q_t the highest *CV* is encountered in some interbedded layers to the left of the profile, close to the CPT cluster to the far right and below the layer boundary to unit III. Generally, the *CV* for q_t is lower than for f_s, suggesting a more confident prediction for q_t. For f_s, the *CV*- values are highest in unit III, but local maxima are as well encountered in the center of the profile between CPT-03 and the CPT-05-08 cluster.

Fig. 10 shows the blindtest predictions for all CPTs in the 2D section both q_t and f_s. Since the measured and predicted CPT-05 to CPT-08 from the CPT cluster are very similar, only CPT-05 is shown as a representative profile. Illustrated are the measured CPTs (black curve), together with the best estimate (q_t: blue, f_s: red) and the three times standard deviation of the prediction.

Fig. 10 which is most relevant for the lateral pile resistance, the prediction falls well within the confidence bounds and can serve readily for design purposes. However, a few parts of the measured CPT are not matched well by the pCPT. The subsequent discussion of the results will focus more in an explanation regarding these outliers, the cause and their potential impact on the design.

It can be seen that the q_t and f_s -estimators approximate the measured values largely well despite the large distances between the CPTs. However, there are also local minima and maxima that are not covered by the simulation. Generally, a good fit is observed in the upper 15 m except for profile CPT-04 where a positive pinch-out in the predicted data and its uncertainty is not covering the measured data. It is to notice that the general shape of the measured profiles close to the mudline is very similar, with limited lateral variations.

CPT-01 shows discrepancies in the prediction of q_t between 15 m and 22 m as well as low f_s, between 12 m and 18 m followed by a good fit which is rather on the conservative side for a pile design.

Large overestimations are seen in CPT-02 below 15 m corresponding to a low resistance layer within the measured CPT. Here, the weak layer is not visible in the acoustic impedance response which shows higher values. Consequently, this leads to a misestimation in the pCPT. Until a depth of 35 m a very good prediction is achieved, despite one underestimation at around 32 m in q_t. Both q_t and f_s show a poor fit between 35 m and 41 m, highly underpredicting the measured values.

Both, the predicted CPT-03 and CPT-04, are generally in good accordance with the measured data. CPT-04 shows despite a generally good fit an overestimation in both q_t and especially for f_s between 22 m and 30 m.

CPT-05 shows a very good fit of q_t to 23 m. Between 23 m and 30 m, both means of q_t and f_s are highly overpredicting the measured data, while the measured data still stays within the uncertainty band. At a depth of about approximately 15 m in both prediction an abrupt increase in uncertainty is observed which correlates with the layer boundary between unit I and unit II. Generally, both CPTs have very similar appearances for the measured and predicted parameters.

In terms of the interpretability of the pCPT profiles, from an engineering perspective underestimating the geotechnical parameters for the here evaluated limit state (SLS - deformation of the monopile) is preferred as it will result in a static substructure design on the safe side, while overestimating is not desirable as it results in an overprediction of the reliability of the system. However, an underestimation of the soil resistance may result in problems during the installation process and fatigue damages or buckling induced during pile driving process, which has also to be accounted for in the design process. Taking CPT-02 at around 16 m as an example, the low measured q_t is indicating a softer deposit. However, the predicted q_t in turn is almost 50 MPa higher than the measured one with the lower bound still being more than 30 MPa higher than the real q_t. Based on the predicted data one would assume a much denser material, which might lead to a less robust design. The opposite is encountered at e.g. CPT-01 in a depth of around 18 m, where the prediction highly underestimates the measured data. Here, a conservative assumption of the strength of the sediment is made which potentially results in a safer design process but in turn might lead to higher costs since the length of the pile may be larger than required.

The predicted results show generally a very good fit in the upper meters. Here the input data is less variable, which can be seen in all measured profiles. In the first meters more consistent marine deposits are encountered at the test side as well as in general in the German North Sea. This makes prediction of the data more reliable, because of less

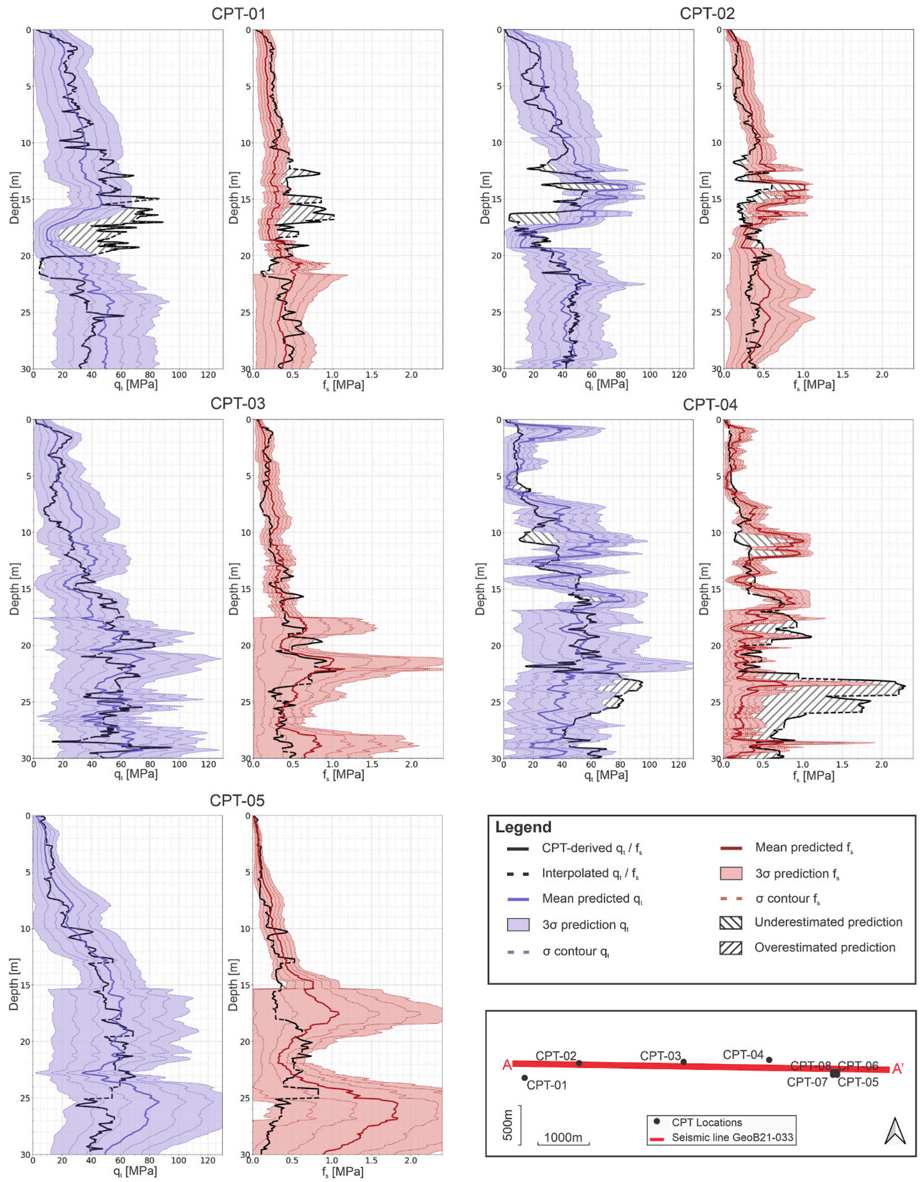

Fig. 10. Comparison of the measured CPT profiles (black) and the predicted blind profiles (blue: q_t; green: f_s), for each CPT along the 2D seismic line. In the right corner a map shows the position of the different CPTs along the seismic line. (For interpretation of the references to color in this figure legend, the reader is referred to the Web version of this article.)

variability leads to less scatter in the computed pCPT field. In other studies it is also seen, that the prediction is more accurate for the upper part of the profiles (e.g. Forsberg et al., 2022; Qu, 2023).

Given the large distances in between the CPTs, local minima and maxima in the measured CPT profiles cannot always be properly replicated by the prediction. Especially, when local anomalies are not seen in adjacent profiles (e.g. CPT-04), they most likely will not be predicted with certainty by the applied method, which is after all a distance-weight-based method considering the CPTs as conditioning data. This is not necessarily a problem with geostatistical methods, but in direct comparison this can be also observed when machine learning is applied to the same type of geotechnical problem (e.g. Sauvin et al., 2019; Siemann et al., 2024).

In different profiles, e.g. CPT-01 between 17 m and 22 m or in CPT-02 between 15 m and 19 m, it appears that low estimated parameters are vertically shifted toward low measured data. This is most likely caused by the fact that the CPTs do not directly lie on the seismic line and have a distance of up to 170 m to the cross-section, causing features seen in the CPT to be vertically shifted due to natural changes in the depth of the deposits.

The larger uncertainties in CPT-05 as part of the CPT clusters, compared to the other CPT profiles, supports the finding of higher uncertainties with increasing distance to measured data points. Additionally, no primary data is available to the right of the cluster location, making the prediction less robust. This also explains the generally very similar results of the CPT profiles, together with the fact that they are very close to each other compared to the rest of the data, which makes the outcome less variable.

The observation that the uncertainty increases with depth is caused by several factors. With increasing depth, less information for the prediction becomes available. While unit I and unit II are fully penetrated by all CPTs, unit III only has CPT-03 reaching deeper, being the only information available after a certain depth. Additionally, the input data itself becomes more variable with depth leading to higher uncertainties in the prediction.

In horizontal direction, uncertainty increases with increasing distance from a measured point and therefore less uncertainty is to be expected if the input data is closely spaced. This is a logical consequence of the variogram introducing more variability with distance. Additionally, more variability apart from the geotechnical site investigations is introduced by more rapid changes in the secondary variable Z_p.

As stated in chapter 3.1.3 the variogram fitting procedure includes subjective uncertainties, especially given the long distances between the different CPT locations. The most sensitive model output is the kriging variance of error which reflects the uncertainty of the prediction. Therefore, changes in the variogram model will also change the magnitude of uncertainty of the prediction which in turn would affect the outcome of the monopile design calculations in chapter 4.2. Anyhow, testing variogram parameters and their effect on the final design outcome was not the main scope of this study. To have a robust study on this, a more complete dataset should be used with more CPTs to be able to construct a more representative experimental variogram.

It can be concluded, that the application of geostatistical simulation works well on the given data set. However, compared to other windfarm areas in the pre-investigation phase, rather many of geotechnical site investigation is available. Here, this method can obtain advantages in contrast to machine learning methods. A direct comparison of different prediction methods in Siemann et al. (2024), did not show a superior method on the given data set. Nevertheless, for more sparsely distributed data, it is expected that data driven methods may show a more robust performance, given that enough training data is available.

The prediction results as shown in Fig. 10 can be used for continuous evaluation of the study area, obtaining advantage against discrete measured points. This can support area-wide decision making in early windfarm development, although care must be always taken regarding the uncertainties attached to it. Considerations for improvement of the CPT prediction are given in the supplementary material section S1.

4.2. Comparison of the derived design pile lengths

The pile lengths were calculated at the CPT locations given in Fig. 10 to allow for a comparison from the blind tests. The discrepancies in vertical direction (compare chapter 4.1) have not been evaluated or corrected. For CPT-01 the detailed results of the calculations are exemplary summarized in Fig. 11. For the other CPTs these graphs are provided in the supplementary material, Figs. S6–S9.

The x-axis in Fig. 11 shows the pile length, while the y-axis shows the percentage of realizations for which $G(X) \geq 0$ for this particular pile length, i.e. for which no failure occurs. The deterministic pile lengths for the approaches MD and QD (s Table 2 and Fig. 7) are drawn as vertical lines. The focus here lies on the probabilistic approach P, for which the *CDF* is displayed in orange.

The pile length calculated by approach MD1, i.e. using the measured CPT, results in the reference length of 25.75 m. In this approach no consideration of any reliability evaluation is included. For CPT-01 the best estimate (mean, approach QD0) of the pCPT results in an almost similar pile length of 25.8 m. From Fig. 10 this may not readily expected, since the pCPT matches well the measured tip resistance in the top 15 m, but underestimates it from 15 m to 20 m and takes a larger value from 20 m downwards. However, for assessing the lateral deformation of the pile, the top third and the bottom third of the pile length (see Supplementary Material Figs. S4–S5) are most influencing the soil-pile interaction. Thus, the underestimation between 15 and 20 m does not play a significant role for this particular case, while the under- and overestimation in the top and bottom third balance each other. The estimations for QD-1, QD-1.645 and QD-2 are on the safe side, i.e. resulting in a larger design pile length. The probabilistic evaluation with a target probability of failure of $1.9{\cdot}10^{-3}$ (99.8 % quantile) results in a pile length of 26.9 m, i.e. on the safe side between -1.0 and -1.645 standard deviations. Compared to the deterministically chosen design profile this leads to a 0.6 m shorter pile and thus a more economic design without reducing the safety.

It is evident, that the results for the quantile values of the pCPT-prediction used as input for the approaches QD p do not match the quantile values of the *CDF* of the pile length. While for the *CDF* realizations accounting for autocorrelation over depth are used, which produce different quantiles of the pCPT-distribution in every depth, the quantile approach uses the same quantile value over the total depth. In using the probabilistic approach the chances are very small that a realization has the same quantile at every depth, whereas the quantile approach produces this explicitly.

A summarized comparison of the results of all CPTs for all methods is shown in Fig. 12. Instead of presenting the actual pile lengths, the difference in pile length in relation to approach MD1 (using the measured CPT) as reference length (red line at $\Delta = 0$ m) is presented. The classification of unsafe ("pile length derived from pCPT is shorter than from the measurement") and safe ("pile length derived from pCPT is longer than from the measurement") is not based on a reliability assessment,

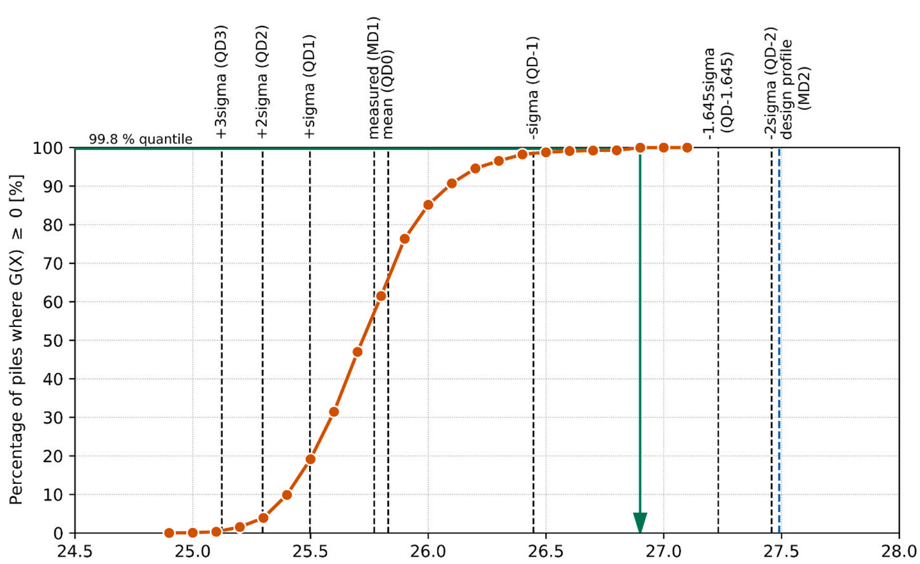

Fig. 11. Calculation results for CPT-01 showing the results for the calculation schemes to derive monopile length presented in Table 2. Deterministic approaches are presented as vertical lines, for the probabilistic approach the CDF is displayed in orange, the design pile length derived as the 99.8 % quantile. (For interpretation of the references to color in this figure legend, the reader is referred to the Web version of this article.)

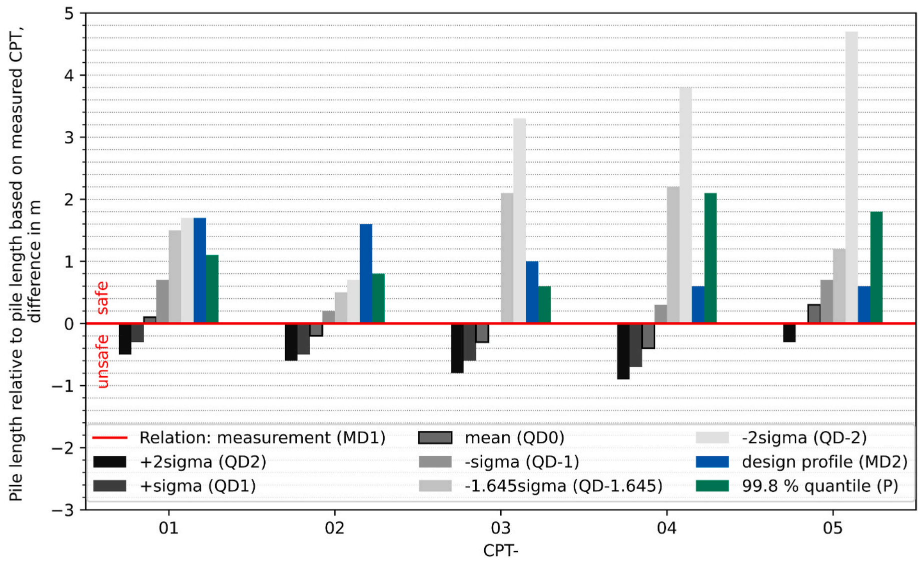

Fig. 12. Difference of pile lengths for the different calculation schemes (see Table 2) in relation to the measured CPT for the different CPT locations, rounded to 10 cm steps.

but is the comparison of the blind test to the measurement. On the x-axis the approaches for every considered CPT are grouped. In gray shades the approaches QD p are depicted. The best estimate (mean - QD0) additionally is bordered with a black line. The blue bar represents the deterministic design profile and the green bar the probabilistic pile length.

The following main observations can be summarized: 1) For every CPT the approaches MD2, QD-1.645, QD-2 and P are on the safe side. 2) For every CPT the approach QD2 is on the unsafe side.

CPT-04 gives the largest difference on the unsafe side for QD0 of −0,4 m, whereas CPT-05 gives it on the safe side with 0.3 m. Comparing to Fig. 10 the reason lies in the over-respectively underestimation of the top 0 to 15 m. For CPT-04 this even overpowers the influence of the large overestimation at the bottom.

It is obvious that neither approach QD0 (mean) nor the approaches QD1 or QD2 should be used for any design calculations. Since the approach QD-1 provides the same result as the measurement for CPT-03, it is also not advisable to use only one standard deviation for a design value. A good deterministic estimate in this case seems to be QD-1.645 with the 5% quantile. As well the probabilistic approach results in a design on the safe side, which is in more than half of the cases also less conservative than the QD-1.645 results. This allows for the conclusion, that the reliability-based design using a stochastic analysis of possible CPT realizations at potential WTA locations not investigated in a geotechnical campaign is a reliable method to assess pile dimensions for a later detailed design and further results here in a more economic design. Hence, the here presented approach is very promising, especially in the earlier phases of an offshore wind project, where WTG positions are not finally decided on yet and relocation of single positions are likely.

5. Conclusion

Geotechnical site investigation campaigns for offshore wind farm design are expensive and scarcely available in early design phases. Using an example from the North Sea a method is presented and validated that combines CPT-data and seismic data as guided variable with a geostatistical co-simulation framework to predict the CPT-tip resistance q_t and sleeve friction f_s at any given location in the field. Despite the large distances between the CPT measurement locations, using the leave-one out assessment the predicted CPT-profiles are in good agreement with the measured data. The application of the predicted CPT-parameters is demonstrated by applying different schemes to the design process of offshore monopile foundations, demonstrated exemplary for the derivation of the design length of the pile under lateral loading. The uncertainty in the CPT-estimates obtained using the prediction methods have been successfully applied using both deterministic and reliability-based design approaches. Especially the use of individual realizations within the reliability-based approach has proven to be promising, since the autocorrelation in the CPT measurements was inherently included and the design pile length can be explicitly linked to a specific target reliability level.

The evaluation of the reliability of the design (safe vs. unsafe) was performed by comparing the computed pile length to the one obtained using the true measured CPT. While the mean value of the CPT prediction as deterministic estimate can produce unsafe designs, it was shown that using the design CPT-Parameters from the 5%-quantile value (−1.645·standard deviations for a normal distribution) or less, the resulting pile length was obtained on the safe side for every investigated CPT location. The optimization of the pile length using the reliability-based design approach for the given target reliability level resulted in a safe estimate of the pile length with respect to the limit state of the horizontal pile head displacement. Hereby the provided uncertainty can be incorporated directly and excessive overdesign could be avoided.

This study included the effect of variability in the soil parameters resulting from the geostatistical interpolation process. Other sources of uncertainty (e.g., measurement, transformation and model uncertainty) have not been included yet. This would however, also affect the evaluation prediction of the CPT profiles. For a definite evaluation of the reliability level and a better comparison with a deterministic design profile by engineering judgement this will be incorporated in future studies. An improvement of the presented calculations is also possible by incorporation of laboratory results and defining soil units before evaluating the pCPTs for every realization. Especially the last point requires closer investigation since a change of the soil unit could, in the case of p-y-curves, result in a different model formulation, which introduce another kind of uncertainty. Also, a handling of the shift of soil layer changes in vertical direction due to the projection on the seismic line should be further investigated. While in the presented cases this effect was proven to be negligible, due to the position and the effect of averaging out over depth, the case may be different for the ULS design criteria such as end bearing or drivability assessment, as for those limit states local minima and maxima at a specific depth (pile tip) are critical. This would be also the case for other offshore foundation systems like jackets. A separate study should be conducted on this topic.

CRediT authorship contribution statement

Lennart Siemann: Writing – review & editing, Writing – original draft, Visualization, Validation, Supervision, Project administration, Methodology, Investigation, Formal analysis, Conceptualization. **Sigrid Wilhelm:** Writing – review & editing, Writing – original draft, Visualization, Validation, Project administration, Methodology, Investigation, Formal analysis, Conceptualization. **Pedram Masoudi:** Writing – review & editing, Validation, Methodology. **Ramiro Relanez:** Writing – review & editing, Visualization, Validation, Investigation. **Patrick Arnold:** Writing – review & editing. **Benjamin Schwarz:** Supervision. **Frank Rackwitz:** Writing – review & editing, Supervision. **Tobias Mörz:** Supervision.

Funding

This work was supported by the Federal Ministry of Economic Affairs and Climate Action under Grant 03 EE3020C (Research project SynCore) and Grant 03EE2050A (Research project ProbPerModel).

Declaration of competing interest

The authors declare that they have no known competing financial interests or personal relationships that could have appeared to influence the work reported in this paper.

Acknowledgment

This study was possible due to the provision of CPT data by RWE (former Innogy), which is very much appreciated.

Appendix A. Supplementary data

Supplementary data to this article can be found online at https://doi.org/10.1016/j.oceaneng.2026.125205.

References

Arnold, P., Kirsch, F., Zorzi, G., 2019. A reliability-based design and optimization procedure for offshore monopile foundations. Proceedings of the 29th European Safety and Reliability Conference (ESREL 2019). Leibnitz University, Hannover, pp. 4263–4270. https://doi.org/10.3850/978-981-11-2724-3_1057-cd.

Arnold, P., Kirsch, F., Kuske, S., Wilhelm, S., 2022. Zur Anwendung probabilistischer Methoden zur Planung von Gründungsstrukturen für Offshore-Windparks am Beispiel von Monopfahlgründungen, vol. 37. Baugrundtagung, Wiesbaden, pp. 171–180.

Atkins, S., Vandeweijer, V., Carpentier, S., Boullenger, B., 2023. Designing convolutional neural networks to make successful predictions of windfarm geotechnical parameters using field geophysical data 2023, 1–5. https://doi.org/10.3997/2214-4609.202321117.

Beyer, S., Dujardin, J., Sauvin, G., Dantal, V., Vanneste, M., Frengstad, B., 2023. Predicting piezocone penetration test response from reflection seismic using machine. Learning 1–5. https://doi.org/10.3997/2214-4609.202320117, 2023.

BSH, 2014. Standard Baugrunderkundung, Mindestanforderungen an die Baugrunderkundung und -untersuchung für Offshore-Windenergieanlagen, Offshore-Stationen und Stromkabel (No. 2. Fortschreibung 5). Hamburg und Rostock.

Caixeta, R.M., Costa, J.F.C.L., 2021. A robust unfolding approach for 3-D domains. Comput. Geosci. 155, 104844. https://doi.org/10.1016/j.cageo.2021.104844.

Carpentier, S., Peuchen, J., Paap, B., Boullenger, B., Meijninger, B., Vandeweijer, V., Kesteren, W.V., Erp, F.V., 2021. Generating synthetic CPTs from marine seismic reflection data using a neural network approach 2021, 1–3. https://doi.org/10.3997/2214-4609.202132008.

Carswell, W., Arwade, S.R., DeGroot, D.J., Lackner, M.A., 2015. Soil–structure reliability of offshore wind turbine monopile foundations. Wind Energy 18, 483–498. https://doi.org/10.1002/we.1710.

Chambers, R.L., Yarus, J.M., Hird, K.B., 2000. Petroleum geostatistics for nongeostaticians Part 2. Lead. Edge 19, 592–599. https://doi.org/10.1190/1.1438664.

Charles, J.A., Gourvenec, S.M., Vardy, M.E., 2022. Coupling site wide CPT profiles and genetic algorithms for whole-site offshore windfarm layout optimization. In: Cone Penetration Testing 2022.

Chautru, J., Binet, H., Masoudi, P., Geffroy, F., Renard, D., 2021. Modeling complex tectonic structures in any kind of grid without space deformation 2021, 1–5. https://doi.org/10.3997/2214-4609.202011541.

Chautru, J.-M., 2024. A geostatistical approach for grid-independent geomodeling in complex tectonic environments. In: Marko Maucec, Dr (Ed.), Applied Spatiotemporal Data Analytics and Machine Learning. IntechOpen, Rijeka. https://doi.org/10.5772/intechopen.115070. Ch. 9.

Chen, J., Vissinga, M., Shen, Y., Hu, S., Beal, E., Newlin, J., 2021. Machine learning–based digital integration of geotechnical and ultrahigh–frequency geophysical data for offshore site characterizations. J. Geotech. Geoenviron. Eng. 147. https://doi.org/10.1061/(ASCE)GT.1943-5606.0002702.

Chiles, J.-P., Delfiner, P., 2012. Geostatistics: Modeling Spatial Uncertainty. John Wiley & Sons.

Ching, J., Lin, G.-H., Chen, J.-R., Phoon, K.-K., 2017. Transformation models for effective friction angle and relative density calibrated based on generic database of coarse-grained soils. Can. Geotech. J. 54 (4), 481–501. https://doi.org/10.1139/cgj-2016-0318.

Cox, P., Boylan, C., Smith, C., Dalgaard, E., Horn, F., Stuyts, B., Bronkhorst, J., Wezenberg, S., Dyer, N., Blacker, K., 2024. AVO-compliant processing and elastic pre-stack inversion of UHRS data at Nederwiek wind farm site I 2024, 1–5. https://doi.org/10.3997/2214-4609.202421096.

Dalgaard, E., Hansen, H.J., Horn, F., Jakobsen, A.F., Kuppens, S., Stuyts, B., 2024. Energy Island - CPT interpretation and soil classification from UHRS pre-stack data 2024, 1–4. https://doi.org/10.3997/2214-4609.202421130.

Damgaard, M., Andersen, L.V., Ibsen, L.B., Toft, H.S., Sørensen, J.D., 2015. A probabilistic analysis of the dynamic response of monopile foundations: soil variability and its consequences. Probab. Eng. Mech. 41, 46–59. https://doi.org/10.1016/j.probengmech.2015.05.001.

Depina, I., 2016. Reliability Analysis of Monopile Foundations for Offshore Wind Turbines.

Depina, I., Hue Le, T.M., Eiksund, G., Benz, T., 2015. Behavior of cyclically loaded monopile foundations for offshore wind turbines in heterogeneous sands. Comput. Geotech. 65, 266–277. https://doi.org/10.1016/j.compgeo.2014.12.015.

Di, H., Pham, N., Abubakar, A., 2023. Estimating geotechnical parameters using semisupervised learning: an example from the Dutch offshore wind farm zone. Geophysics 89, WA85–WA93. https://doi.org/10.1190/geo2023-0054.1.

DIN 1055-2:2010-11, 2010. DIN 1055-2:2010-11: Einwirkungen auf Tragwerke - Teil 2: Bodenkenngrößen. Beuth Verlag.

DIN 4020:2010-12, 2010. Geotechnische Untersuchungen für bautechnische Zwecke – Ergänzende Regelungen zu DIN EN 1997-2. Beuth Verlag.

DIN, E.N., 1990–2021. DIN EN 1990: Eurocode: Grundlagen der Tragwerksplanung; Deutsche Fassung EN 1990:3002 + A1:2005 + A1:2005/AC:2010. Beuth Verlag.

DIN EN 1997-2:2010-10, 2010. Eurocode 7 – Entwurf, Berechnung und Bemessung in der Geotechnik – Teil 2: Erkundung und Untersuchung des Baugrunds; Deutsche Fassung EN 1997-2:2007 + AC:2010. Beuth Verlag.

El Haj, A.-K., Soubra, A.-H., Fajoui, J., 2019. Probabilistic analysis of an offshore monopile foundation taking into account the soil spatial variability. Comput. Geotech. 106, 205–216. https://doi.org/10.1016/j.compgeo.2018.10.011.

Forsberg, C.F., Sauvin, G., Klingvort, R.T., Vardy, M.E., Vanneste, M., Kort, A., 2022. Integrated Ground Model - Ten noorden van de Waddeneilanden Wind Farm Zone (Ministerie van Economische Zaken en Klimaat, Rijksdienst voor Ondernemend Nederland) (No. No. 20190798-04-R). Notwegian Geotechnical Institute, Oslo, Norway.

Fuglstad, G.-A., Lindgren, F., Simpson, D., Rue, H., 2015. Exploring a new class of non-stationary spatial Gaussian random fields with varying local anisotropy. Stat. Sin. 115–133. https://doi.org/10.5705/ss.2013.106w.

Goodman, S., Krom, T., Giovacchini, F., Grove, M., Bodger, B., Hollingsworth, A., Ward, O., Nicholls, C., 2021. An agile, automated and repeatable multi-disciplinary approach to integrated ground modelling for offshore windfarm. development 1–5. https://doi.org/10.3997/2214-4609.202121051, 2021.

Grafarend, E.W., Zwanzig, S., Awange, J.L., 2022. Applications of linear and nonlinear models - fixed effects. Random Effects, and Total Least Squares. Springer Geophysics. Springer, Cham. https://doi.org/10.1007/978-3-030-94598-5.

Gringarten, E., Deutsch, C.V., 2001. Teacher's aide variogram interpretation and modeling. Math. Geol. 33, 507–534. https://doi.org/10.1023/A:1011093014141.

Horn, F., Hansen, H., Jakobsen, A., Kuppens, S., Stuyts, B., Dalgaard, E., 2023. Energy Island North Sea - Seismic Geotechnical Interpretation of Seismic Dual Setup. Copenhagen.

Huang, J., Kelly, R., Li, D., Zhou, C., Sloan, S., 2016. Updating reliability of single piles and pile groups by load tests. Comput. Geotech. 73, 221–230. https://doi.org/10.1016/j.compgeo.2015.12.003.

Isatis.neo TM, 2024. Geostatistical software. Geovariances, a Datamine company.

ISO 19901-4:2025(en), 2025. Oil and Gas Industries Including Lower Carbon Energy - Specific Requirements for Offshore Structures - Part 4: Geotechnical Design Considerations, Third Edition 2025-02, ISO 2025, SwitzerlandJournel, A.G., Huijbregts, C.J., 2003. Mining Geostatistics. Blackburn Press.

Karkov, K.H., Dalgaard, A.T., Diaz, A.T., Duarte, H., Hansen, H.J., Hviid, S., Hoegh van Gilse, N.C., Krogh, L., Kuppens, S., Salaün, G., 2022. Case study: AVO inversion and processing of ultra-high resolution seismic for a windfarm application. Presented at the EAGE Annual 83rd Conference and Exhibition. Madrid.

Keil, H., Hepp, D., Andresen, K., 2021. Changing North Sea, Cruise No. HE569, February 03 - February 27, 2021, Bremerhaven (Germany) - Bremerhaven (Germany). Gutachterpanel Forschungsschiffe. https://doi.org/10.48433/cr_he569. Bonn.

Kulhawy, F.H., Mayne, P.W., 1990. Manual on Estimating Soil Properties for Foundation Design. No. EL-6800). New York.

Lemaire, M., Chateauneuf, A., Mitteau, jean-C., 2009. Structural Reliability.

Lesny, K., 2008. Gründung von Offshore-Windenergieanlagen – Entscheidungshilfen für Entwurf und Bemessung. Bautechnik 85, 503–511. https://doi.org/10.1002/bate.200810037.
Lindgren, F., Rue, H., Lindström, J., 2011. An explicit link between Gaussian fields and Gaussian Markov random fields: the stochastic partial differential equation approach. J. Roy. Stat. Soc. B 73, 423–498. https://doi.org/10.1111/j.1467-9868.2011.00777.x.
Lohrberg, A., Krastel, S., Unverricht, D., Schwarzer, K., 2022a. The heligoland glacitectonic complex in the southeastern North Sea: indicators of a pre- or early-Elsterian ice margin. Boreas 51, 100–117. https://doi.org/10.1111/bor.12551.
Lohrberg, A., Schneider von Deimling, J., Grob, H., Lenz, K.-F., Krastel, S., 2022b. Tunnel valleys in the southeastern North Sea: more data, more complexity. E&G Quaternary Science Journal 71, 267–274.
Masoudi, P., 2022. Fuzzy membership function for weighting pairs in variographical analysis. Spatial Statistics 52, 100717. https://doi.org/10.1016/j.spasta.2022.100717.
Masoudi, P., Binet, H., Simon, C., Pelletier, B., Faucheux, C., Rambert, F., Assy, Y., 2024. 3D modelling of standard penetration test in the framework of assessing liquefaction risk 2024, 1–5. https://doi.org/10.3997/2214-4609.202430031.
Masoudi, P., Binet, H., Simon, C., Pelletier, B., Rambert, F., Assy, Y., 2023. Improving seismic velocity mapping using standard penetration test data in a cokriging interpolation 2023, 1–5. https://doi.org/10.3997/2214-4609.202320067.
Masoudi, P., Simon, C., Faucheux, C., Blanckaert, M., Binet, H., 2025. (accepted with minor revision). Stratigraphical and geotechnical modelling by geostatistics, applied to penetrometer and Menard pressure-meter tests. Math. Geosci. https://doi.org/10.1007/s11004-025-10242-0.
Matheron, G., 1973. The intrinsic random functions and their applications. Adv. Appl. Probab. 5, 439–468.
Mayne, P.W., Peuchen, J., 2018. Evaluation of CPTU Nkt Cone Factor for Undrained Strength of Clays. Cone Penetration Testing 2018 (Delft). CRC, pp. 423–429.
Melchers, R.E., 1999. Structural Reliability Analysis and Prediction. John Wiley Sons Ltd., Chichester, England.
Peignard, L., Masoudi, P., Binet, H., 2024. Reservoir gross rock volume estimation of a gently dipping structural trap. Using Geostatistical Time-Depth Conversion Method 1–5. https://doi.org/10.3997/2214-4609.202421041, 2024.
Pula, W., 2007. Reliability of laterally loaded rigid piles. In: Griffiths, D.V., Fenton, GordonA. (Eds.), Probabilistic Methods in Geotechnical Engineering. Springer, Vienna, Vienna, pp. 169–183. https://doi.org/10.1007/978-3-211-73366-0_7.
Pyrcz, M.J., Deutsch, C.V., 2014. Geostatistical Reservoir Modeling. Oxford University Press, USA.
Qu, D., 2023. Machine learning-based synthetic CPT prediction in offshore windfarms with sparse data 2023, 1–5. https://doi.org/10.3997/2214-4609.202321126.
RFEM 6, 2022. *Structural Analysis and Design Software* (Version 6.05.0004) with Web Service. Dlubal Software GmbH, Tiefenbach, Germany. Retrieved from, version 1.18.0. https://www.dlubal.com.
Robertson, P.K., 2009. Interpretation of cone penetration tests — a unified approach. Can. Geotech. J. 46, 1337–1355. https://doi.org/10.1139/T09-065.
Robertson, P.K., Cabal, K., 2022. Guide to Cone Penetration Testing, seventh edition.
Sauvin, Guillaume, Vanneste, M., Klinkvort, R.T., Dujardin, J., Forsberg, C., 2022b. Towards integrated ground models - an example from TNW Offshore windfarm. Presented at the EAGE Annual - 83rd Conference & Exibition. Madrid, Spain.
Sauvin, G., Vanneste, M., Vardy, M., Klinkvort, R.T., Forsberg, C., 2019. Machine learning and quantitative ground models for improving offshore wind site characterization. https://doi.org/10.4043/29351-MS.
Sauvin, G., Vardy, M., Klinkvort, R.T., Vanneste, M., Forsberg, C.F., Kort, A., 2022. State-of-the-Art ground model development for offshore renewables – TNW case study 2022, 1–5. https://doi.org/10.3997/2214-4609.202221109.
Savidis, S., Richter, T., Kirsch, F., Rücker, W., 2018. Entwurf und Bemessung von Gründungen für Offshore-Windenergieanlagen. In: Grundbau-Taschenbuch- Teil 3: Gründungen und Geotechnische Bauwerke. Wilhelm Ernst & Sohn Verlag für Architektur und technische Wissenschaften GmbH & Co. KG, Berlin.
Shoukat, G., Michel, G., Coughlan, M., Malekjafarian, A., Thusyanthan, I., Desmond, C., Pakrashi, V., 2023. Generation of synthetic CPTs with access to limited geotechnical data for offshore sites. Energies 16. https://doi.org/10.3390/en16093817.
Siemann, L., Masoudi, P., Maraka, R., Opris, R., Pande, Y., Römer-Stange, N., Morales, N., Mörz, T., 2024. Comparison of different prediction methods to derive synthetic CPT profiles - an offshore wind farm case study from the German North Sea. Presented at the 7th International Conference on Geotechnical and Geophysical Site Characterization. Barcelona. https://doi.org/10.23967/isc.2024.233.
Siemann, L., Morales, N., Chautru, J.M., Pein, T., 2022. Prediction and probability estimation of geotechnical parameters for offshore windfarm site characterization using geostatistical simulation 2022, 1–5. https://doi.org/10.3997/2214-4609.202221076.
Silva, D.S.F., Boisvert, J., 2014. Mineral Resource Classification: a Comparison of New and Existing Techniques, 114. Journal of the Southern African Institute of Mining and Metallurgy, pp. 265–273.
Sullivan, W.R., Reese, L.C., Fenske, C.W., 1980. Unified method for analysis of laterally loaded piles in clay. In: Numerical Methods in Offshore Piling, pp. 135–146. https://doi.org/10.1680/nmiop.00865.0017.
Tandjiria, V., Teh, C.I., Low, B.K., 2000. Reliability analysis of laterally loaded piles using response surface methods. Struct. Saf. 22, 335–355. https://doi.org/10.1016/S0167-4730(00)00019-9.
Vanneste, M., Sauvin, G., Dujardin, J.-R., Forsberg, Carl, Klinkvort, R.T., Forsberg, Cathinka, Hansen, R., 2022. Data-driven ground models: the road to fully-integrated site characterization and design, 3–21. https://doi.org/10.1007/978-981-16-7735-9_1.
Vardy, M.E., Vanneste, M., Henstock, T.J., Clare, M.A., Forsberg, C.F., Provenzano, G., 2017. State-of-the-art remote characterization of shallow marine sediments: the road to a fully integrated solution. Near Surf. Geophys. 15, 387–402. https://doi.org/10.3997/1873-0604.2017024.
Vardy, M.E., Clare, M.A., Vanneste, M., Forsberg, C.F., Dix, J.K., 2018. Seismic inversion for site characterization: when, where and why should we use it? Presented at the Offshore Technology Conference https://doi.org/10.4043/28730-MS D021S027R005.
Verly, G., Parker, H.M., 2021. Conditional simulation for mineral resource classification and mining dilution assessment from the early 1990s to now. Math. Geosci. 53, 279–300. https://doi.org/10.1007/s11004-021-09924-2.
Vrouwenvelder, T., Dimova, S., Sousa, L.M., Marková, J., Mancini, G., Kuhlmann, U., Taras, A., Jockwer, R., Jäger, W., Schweckendiek, T., Franchin, P., Skejić, D., Sørensen, J.D., Spehl, P., Stacy, M., Feldmann, M., Croce, P., Zhao, B., Tanner, P., Knippers, J., Mollaert, M., André, J., Steenbergen, R., Kohler, J., Bakeer, T., Maljaars, J., Allaix, D., Spross, J., 2024. Reliability Background of the Eurocodes – Support to the Implementation, Harmonization and Further Development of the Eurocodes. Publications Office of the European Union. https://doi.org/10.2760/9482837.
Wackernagel, H., 2003. Multivariate Geostatistics: an Introduction with Applications. Springer Science & Business Media.
Wichtmann, T., Kimmig, I., Triantafyllidis, T., 2017. On correlations between "dynamic" (small-strain) and "static" (large-strain) stiffness moduli – an experimental investigation on 19 sands and gravels. Soil Dynam. Earthq. Eng. 98, 72–83. https://doi.org/10.1016/j.soildyn.2017.03.032.
Winsemann, J., Koopmann, H., Tanner, D.C., Lutz, R., Lang, J., Brandes, C., Gaedicke, C., 2020. Seismic interpretation and structural restoration of the Heligoland glaciotectonic thrust-fault complex: implications for multiple deformation during (pre-)Elsterian to Warthian ice advances into the southern North sea Basin. Quat. Sci. Rev. 227, 106068. https://doi.org/10.1016/j.quascirev.2019.106068.
Wu, X., 2017. Building 3D subsurface models conforming to seismic structural and stratigraphic features. Geophysics 82, IM21–IM30. https://doi.org/10.1190/geo2016-0255.1.
Zhao, C., Gong, W., Juang, C.H., Tang, H., Hu, X., Li, Z., 2024. Probabilistic analysis of lateral behaviour of offshore wind turbine monopile considering uncertainties of geological model and loads. Comput. Geotech. 171, 106348. https://doi.org/10.1016/j.compgeo.2024.106348.
Zorzi, G., Mankar, A., Velarde, J., Sørensen, J.D., Arnold, P., Kirsch, F., 2020. Reliability analysis of offshore wind turbine foundations under lateral cyclic loading. Wind Energy Science 5, 1521–1535. https://doi.org/10.5194/wes-5-1521-2020.